# Transition from two-dimensional to three-dimensional magnetohydrodynamic turbulence

## ANDRÉ THESS[1] AND OLEG ZIKANOV[2]

[1]Department of Mechanical Engineering, Ilmenau University of Technology,
P. O. Box 100565, 98684 Ilmenau, Germany

[2]Department of Mechanical Engineering, University of Michigan-Dearborn,
4901 Evergreen Road, Dearborn, MI 48128-1491, USA

We report a theoretical investigation of the robustness of two-dimensional inviscid magnetohydrodynamic (MHD) flows at low magnetic Reynolds numbers with respect to three-dimensional perturbations. We use a combination of linear stability analysis and direct numerical simulations to analyse three problems, namely the flow in the interior of a triaxial ellipsoid, and two unbounded flows: a vortex with elliptical streamlines and a vortex sheet parallel to the magnetic field. The flow in a triaxial ellipsoid is found to present an exact analytical model which demonstrates both the existence of inviscid unstable three-dimensional modes and the stabilizing role of the magnetic field. The nonlinear evolution of the flow is characterized by intermittency typical of other MHD flows with long periods of nearly two-dimensional behaviour interrupted by violent three-dimensional transients triggered by the instability. We demonstrate, using the second model, that motion with elliptical streamlines perpendicular to the magnetic field becomes unstable with respect to the elliptical instability once the magnetic interaction parameter falls below a critical magnitude whose value tends to infinity as the eccentricity of the streamlines increases. Furthermore, the third model indicates that vortex sheets parallel to the magnetic field, which are unstable for any velocity and any magnetic field, emit eddies with vorticity perpendicular to the magnetic field. Whether the investigated instabilities persist in the presence of small but finite viscosity, in which case two-dimensional turbulence would represent a singular state of MHD flows, remains an open question.

## 1. Introduction

### 1.1. *Motivation*

Turbulent flows of liquid metals under the influence of magnetic fields occur under a wide range of circumstances, ranging from metallurgy (Davidson 1999) and fundamental turbulence research (Moreau 1990; Tsinober 2001) to the movement of the Earth's inner core (Moffatt 1978). It is widely accepted that when the magnetic Reynolds number $Rm$ (to be defined below) is small, and the magnetic field is sufficiently strong, homogeneous magnetohydrodynamic (MHD) turbulence becomes nearly two-dimensional and the electromagnetic dissipation of kinetic energy is weak. Such a situation is sometimes modelled using purely two-dimensional equations in which the electromagnetic energy dissipation vanishes. The purpose of the present paper is to
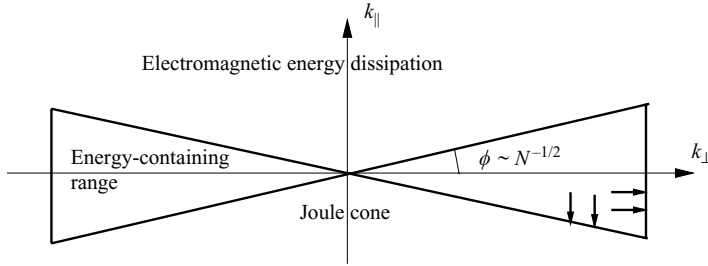
FIGURE 1. Distribution of kinetic energy at $N \gg 1$.

critically assess this approach in an investigation of stability of structures typically observed in two-dimensional flows with respect to three-dimensional perturbations.

Let us start by discussing the issue at the centre of our study in some detail. When an incompressible fluid with density $\rho$, kinematic viscosity $\nu$, electrical conductivity $\sigma$, and permeability $\mu_0$ moves with velocity $U$ and characteristic length scale $L$ in a uniform magnetic field $B$, and when the magnetic Reynolds number $Rm = \mu_0 \sigma U L$ is small, the state of the flow is characterized by the Reynolds number and the electromagnetic interaction parameter defined respectively as

$$Re \equiv \frac{UL}{\nu}, \quad N \equiv \frac{\sigma B^2 L}{\rho U}. \tag{1.1}$$

We are interested in fully developed turbulence ($Re \to \infty$) under a strong magnetic field $N \gg 1$. It has been established by Moffatt (1967) (see also Davidson 1997) and confirmed experimentally by Alemany *et al.* (1979) and numerically by Schumann (1976), Zikanov & Thess (1998), Knaepen & Moin (2004) that the turbulent flow tends to become anisotropic and to develop flow structures which are elongated along the magnetic field so as to avoid electromagnetic (Joule) dissipation. It is arguable whether or not the flow can finally attain a purely two-dimensional form with no variations along the magnetic field and with zero Joule dissipation. In reality, one is always left with a quasi-two-dimensional flow because of confining walls, where Hartmann boundary layers develop (Sommeria 1986), or because of highly elongated structures which are not suppressed. Sommeria & Moreau (1982) have aptly summarized our conceptual understanding of MHD turbulence at $N \gg 1$ by characterizing the distribution of kinetic energy among the wavenumbers $k_\perp$ and $k_\parallel$ perpendicular and parallel to the magnetic field, respectively. This distribution of kinetic energy in the state of so-called 'quasi-two-dimensional turbulence' is sketched in figure 1. For $N \gg 1$ the kinetic energy of the flow is confined to a narrow region in the wavenumber space, outside the 'Joule cone' in which electromagnetic energy dissipation takes place and below those wavenumbers $k_\perp$ for which viscous dissipation dominates. The angle $\phi \sim N^{-1/2}$ of the energy-containing region shrinks to zero as $N \to \infty$. This picture can lead to the assumption that for the idealized case of the flow in an unbounded domain and for sufficiently strong magnetic field quasi-two-dimensional MHD turbulence becomes purely two-dimensional and the Joule energy dissipation vanishes.

However, there have been strong experimental and numerical indications that this assumption does not hold. In their experiments on freely decaying homogeneous MHD turbulence in mercury Alemany *et al.* (1979) and Caperan & Alemany (1985) found that variations of the velocity fluctuations along the applied magnetic field and strong Joule dissipation persisted even at high interaction parameters. Disagreements

between drag measurements of MHD flows in channels with very large aspect ratios (low influence of Hartmann walls) (Tsinober 1990) and purely two-dimensional numerical simulations of turbulent channel flow by Jimenez (1990) give rise to serious doubts whether quasi-two-dimensional turbulence is close to purely-two-dimensional turbulence. Direct numerical simulations of forced MHD turbulence by Zikanov & Thess (1998), albeit restricted to moderate interaction parameters, indicated that two-dimensional vortices, once they have formed, may undergo violent three-dimensional instabilities resulting in an intermittent behaviour. Experimental (Lahjomri, Caperan & Alemany 1993) and numerical (Mutschke *et al.* 2001) investigations of a flow around a cylinder under the influence of a magnetic field parallel to the incoming flow have shown that three-dimensional instabilities persist for strong magnetic fields. Finally, numerical simulations of MHD turbulence subject to a two-dimensional forcing, which have been carried out by Nakauchi, Oshima & Saito (1992) using an EDQNM model, have provided evidence that even for very high values of the interaction parameter and strong non-isotropy of the flow, the Joule energy dissipation of the flow tends to a non-zero finite value.

The foregoing observations show that a purely two-dimensional state is hard to achieve by an MHD flow (if it is achievable at all) even if there are no confining Hartmann walls. This is obviously due to the survival of perturbations with large length scales along the magnetic field. The difficulty in establishing a purely two-dimensional MHD flow can be considered from two different viewpoints. One can say that the magnetic field was not strong enough to make the flows entirely two-dimensional in the experiments and simulations mentioned. Alternatively, one can hypothesize that the magnetic field is, in principle, unable to suppress the always present instability of two-dimensional flows to three-dimensional perturbations.

In the present paper we therefore investigate the robustness of purely two-dimensional turbulence using stability theory combined with direct numerical simulations. We emphasize at the outset that our stability analysis is entirely inviscid. Very high Reynolds number $Re = 10^6$ is used in the nonlinear simulations. The molecular viscosity together with the numerical viscosity of the scheme add some dissipation but, since only the initial stages of instability are simulated, the flows can be considered essentially inviscid. The assumption of zero viscosity makes our stability problems amenable to rigorous analytic treatment which would not be the case if we had added viscosity. We are aware that one should be wary of drawing far-reaching conclusions based on inviscid stability theory since, as in the case of the magnetorotational instability in sheared or differentially rotating fluids (Balbus & Hawley 1998), viscosity may provide a cutoff at small scales.

Our presentation is organized as follows. In the following section we start our discussion with the consideration of a flow in a triaxial ellipsoid by deriving an exact low-dimensional model for a flow at $Rm \ll 1$. This model, in spite of its simplicity and limitation to a narrow class of flows, illustrates the main ideas of our work. In §3 we formulate the general stability problem for two-dimensional flows in an unbounded domain and identify those structures, namely elliptical vortices and vortex sheets, which play a key role in the transition from two-dimensional to three-dimensional behaviour at high Reynolds number. Section 4 contains an analysis of the linear stability of a single unbounded vortex with elliptical streamlines, which can be carried out almost entirely analytically, and identifies the elliptical instability (Kerswell 2002) as one mechanism for the formation of three-dimensional structures in MHD. The instability is further investigated in full three-dimensional nonlinear simulations of a spatially limited vortex. In §5 we discuss the Kelvin–Helmholtz instability of vortex

sheets when the basic flow is parallel to the magnetic field. In §6, we summarize our conclusions and discuss some open questions which would be useful to investigate in future.

### 1.2. *On the proper definition of the magnetic interaction parameter*

Our stability analyses to be presented below will be performed for an inviscid fluid, corresponding to $Re \to \infty$. Hence the magnetic interaction parameter $N$ will be the only remaining dimensionless group and it is important to define it in such a way that it reflects the intrinsic properties of the instabilities.

There are two possible approaches to the definition. One is to formally apply the formula (1.1) with $L$ and $U$ being the typical length and velocity scales in some real or imaginary 'reference' state of the flow. This approach was followed in the majority of earlier investigations. One particular example is the numerical simulations by Schumann (1976), Zikanov & Thess (1998), or Knaepen & Moin (2004), where the reference state was the isotropic state immediately before the application of the magnetic field. Defined in this way, the parameter does not reflect the transformation of the flow caused by the imposed magnetic field but, rather, identifies the flow evolution at given external conditions (size of the flow domain, properties of the fluid, and the strength of the magnetic field).

Another way is to consider $N$ as a measure of the ratio between the Lorentz force and inertia forces at any given moment of the flow evolution. In this case, one has to take into account that the strength of the Lorentz force is determined by the magnitude of the gradient of velocity in the direction of the magnetic field. As the flow transforms into anisotropic state, the Lorentz force and, thus, the effective value of $N$ decreases. For example, one can formally estimate the ratio between the Lorentz and inertia forces as (see (3.1) in this paper and discussion in Vorobev *et al.* 2005)

$$N_{eff} \equiv \frac{\sigma B^2}{\rho U} \frac{L^3}{L_{\parallel}^2}, \tag{1.2}$$

where $L_{\parallel}$ is the current length scale in the direction of the magnetic field.

Although reflecting the fact that the Lorentz force becomes weaker in anisotropic flows and disappears in purely two-dimensional flows, the definition (1.2) does not provide an unambiguous identification of a flow in the entirety of its evolution. Furthermore, it put us in an awkward position of dealing with a constantly changing governing parameter. For these reasons, we follow the more traditional definition (1.1) in this paper.

In the problems without a well-defined length scale $L$, such as those considered in §§2 and 4 of this paper, another definition of the interaction parameter is required. Considering $N$ as a ratio between the typical eddy turnover time $T$ and the Joule damping time $\tau \equiv \rho/\sigma B^2$ and estimating $T$ as $\omega^{-1}$, where $\omega$ is the typical vorticity, one arrives at

$$N_{vort} \equiv \frac{\sigma B^2}{\rho \omega}. \tag{1.3}$$

This definition can be rendered consistent with (1.1) or (1.2) depending on whether the reference or current value of $\omega$ is used. In this paper, we employ the first strategy, the reference state being the basic state, the linear or nonlinear instability of which is investigated.

Yet another definition of the magnetic interaction parameter is required when considering the problem of linear stability of a vortex sheet of zero thickness in §5.1.

In this case, the basic flow lacks well-defined scales of both length and vorticity. The only possible definition is

$$N \equiv \frac{\sigma B^2}{\rho U_0 k} \tag{1.4}$$

based on the velocity of the basic flow $U_0$ and the reciprocal wavenumber $k^{-1}$ of the perturbation as the velocity and length scales.

## 2. Instability in a bounded domain

### 2.1. *An exact solution for inviscid MHD flow in a triaxial ellipsoid*

Consider an inviscid electrically conducting incompressible fluid which is confined to the interior of the electrically insulating triaxial ellipsoid

$$\frac{x^2}{a^2} + \frac{y^2}{b^2} + \frac{z^2}{c^2} = 1, \tag{2.1}$$

and subjected to the influence of a homogeneous magnetic field $\boldsymbol{B} = B\boldsymbol{e}_z$. If the magnetic Reynolds number $Rm$ defined in the previous section is small, the dynamics of the flow is governed by the equations

$$\frac{\partial \boldsymbol{v}}{\partial t} + (\boldsymbol{v} \cdot \nabla)\boldsymbol{v} = -\frac{1}{\rho}\nabla p + \frac{1}{\rho}\boldsymbol{J} \times \boldsymbol{B}, \quad \nabla \cdot \boldsymbol{v} = 0, \tag{2.2}$$

$$\boldsymbol{J} = \sigma(-\nabla\phi + \boldsymbol{v} \times \boldsymbol{B}), \quad \nabla \cdot \boldsymbol{J} = 0, \tag{2.3}$$

where $\boldsymbol{J}$ is the electric current density and $\phi$ the electric potential (Roberts 1967; Moreau 1990; Davidson 2001). The justification to neglect the magnetic field $\boldsymbol{b}$ associated with the eddy currents $\boldsymbol{J}$ (where $\boldsymbol{J} = \mu_0^{-1}\nabla \times \boldsymbol{b}$) comes from the fact that its magnitude $b \sim \mu_0 J L \sim \mu_0 \sigma v L B$ is smaller than the magnitude of the applied field by a factor $Rm$; for a liquid metal under laboratory conditions we have $\sigma \approx 10^6\,\Omega^{-1}\,\mathrm{m}^{-1}$, $v \approx 0.1\,\mathrm{m\,s}^{-1}$, $L \approx 0.1$ m and thus $Rm \approx 0.01$. The equations are supplemented by the boundary conditions

$$\boldsymbol{v} \cdot \boldsymbol{n} = \boldsymbol{J} \cdot \boldsymbol{n} = 0 \tag{2.4}$$

where $\boldsymbol{n}$ denotes the unit vector normal to the surface of the ellipsoid. The first of these is the free-slip boundary condition for the velocity which implies that the wall can exert no tangential stress on the (inviscid) fluid. The second boundary condition expresses that no electric current can leave the fluid since the ellipsoid is assumed to be electrically insulating. The electrical boundary conditions are known to play an important role in MHD flows at low $Rm$ (see Dormy, Cardin & Jault 1998; Dormy, Jault & Soward 2002; Hollerbach & Skinner 2001). It would have been interesting therefore to study the present problem for a wall with arbitrary conductivity. This general case, however, is not amenable to rigorous analytic treatment and will therefore not be considered here.

If there is no magnetic field, there exists a family of three-dimensional time-dependent velocity distributions of the form

$$\boldsymbol{v}(x, y, z, t) = U(t)\left[y\frac{c}{b}\boldsymbol{e}_z - z\frac{b}{c}\boldsymbol{e}_y\right] + V(t)\left[z\frac{a}{c}\boldsymbol{e}_x - x\frac{c}{a}\boldsymbol{e}_z\right] + W(t)\left[x\frac{b}{a}\boldsymbol{e}_y - y\frac{a}{b}\boldsymbol{e}_x\right]. \tag{2.5}$$

They are exact solutions to the Euler equations provided that the set of coefficients $(U, V, W)$ satisfies three nonlinear ordinary differential equations, which

are mathematically identical to the equations describing the free rotation of a solid body (Gledzer & Ponomarev 1977; Gledzer, Dolzhansky & Obukhov 1981; Kerswell 2002). The velocity field described by (2.5) automatically satisfies the incompressibility constraint, the free-slip condition, and is a superposition of three basic two-dimensional flows. Each of them has elliptical streamlines and a spatially uniform vorticity directed along the axis of the ellipsoid which is perpendicular to the plane of motion. Notice that $U$, $V$, and $W$ have the dimensions of vorticity, not velocity.

We extend the existing theory to the case when a magnetic field is present by expressing the electric current density in the form

$$\boldsymbol{J}(x, y, z, t) = I(t) \left[ y \frac{c}{b} \boldsymbol{e}_z - z \frac{b}{c} \boldsymbol{e}_y \right] + J(t) \left[ z \frac{a}{c} \boldsymbol{e}_x - x \frac{c}{a} \boldsymbol{e}_z \right] + K(t) \left[ x \frac{b}{a} \boldsymbol{e}_y - y \frac{a}{b} \boldsymbol{e}_x \right] \tag{2.6}$$

which satisfies the condition $\nabla \cdot \boldsymbol{J} = 0$ as well as the electric boundary condition (2.4). The coefficients $I, J, K$ describe the strength of eddy currents induced by the movement of the fluid in the magnetic field. Notice that $I$, $J$, and $K$ have the dimensions $\mathrm{A\,m^{-3}}$, i.e. current density per metre. If the fluid rotates around the $x$-axis ($U \neq 0, V = 0, W = 0$), the induced current is in the $(x, z)$-plane ($I = 0, J \neq 0, K = 0$), and its strength is proportional to the magnetic field and the intensity of the flow. We may therefore expect that $J \sim BU$. By the same token it may be anticipated that $I \sim BV$ for a rotation around the $y$-axis, while for rotation around the $z$-axis the electromotive force is likely to be balanced by an electric potential gradient which leads to the hypothesis $K = 0$.

In order to express $(I, J, K)$ through $(U, V, W)$ we take the curl of Ohm's law (2.3), which gives $\nabla \times (\boldsymbol{v} \times \boldsymbol{B}) = \nabla \times \boldsymbol{J}/\sigma$ and invoke the representations (2.5) and (2.6). This provides us, after some algebra, with the desired relations $I = \sigma BVab/(b^2 + c^2)$, $J = -\sigma BUab/(a^2 + c^2)$, $K = 0$ for the amplitudes of the eddy currents. Notice that it is not necessary to compute the electric potential explicitly. However, one can readily integrate (2.3) for $\phi$ in order to verify that the computed electric current density is indeed correct. We now eliminate the pressure by taking the curl of equation (2.2). Observing that the vorticity $\boldsymbol{\omega} = \nabla \times \boldsymbol{v}$ corresponding to the velocity field (2.5) has the form

$$\boldsymbol{\omega} = U \cdot \left( \frac{b}{c} + \frac{c}{b} \right) \boldsymbol{e}_x + V \cdot \left( \frac{a}{c} + \frac{c}{a} \right) \boldsymbol{e}_y + W \cdot \left( \frac{a}{b} + \frac{b}{a} \right) \boldsymbol{e}_z \tag{2.7}$$

and is spatially uniform, it follows that $(\boldsymbol{v} \cdot \nabla)\boldsymbol{\omega} = \boldsymbol{0}$ and the vorticity equation becomes

$$\frac{\partial \boldsymbol{\omega}}{\partial t} = (\boldsymbol{\omega} \cdot \nabla)\boldsymbol{v} + \frac{1}{\rho} \nabla \times (\boldsymbol{J} \times \boldsymbol{B}). \tag{2.8}$$

Inserting the expressions for $\boldsymbol{v}$, $\boldsymbol{\omega}$, $\boldsymbol{J}$, and $\boldsymbol{B}$ it is readily shown that they are exact solutions to the vorticity equation provided that the coefficients $U, V, W$ obey the equations

$$(b^2 + c^2)\dot{U} = (b^2 - c^2)VW - \frac{\sigma B^2}{\rho} \left( \frac{a^2 b^2}{a^2 + c^2} \right) U, \tag{2.9}$$

$$(c^2 + a^2)\dot{V} = (c^2 - a^2)UW - \frac{\sigma B^2}{\rho} \left( \frac{a^2 b^2}{b^2 + c^2} \right) V, \tag{2.10}$$

$$(a^2 + b^2)\dot{W} = (a^2 - b^2)UV. \tag{2.11}$$

It should be emphasized that the derivation of this system from the governing equations (2.2) and (2.3) did not involve any approximation.

The system (2.9)–(2.10) can be made non-dimensional by introducing dimensionless variables according to $(U, V, W) = \alpha(U_*, V_*, W_*)$ and $t = t_*/\alpha$ where $\alpha = (\sigma B^2/\rho)a^2b^2/[(a^2 + c^2)(b^2 + c^2)]$ is the inverse of the Joule decay time. Using the abbreviations $A = a/c$ and $B = b/c$ and dropping the asterisk the equations become

$$\dot{U} = \frac{B^2 - 1}{B^2 + 1} VW - U, \tag{2.12}$$

$$\dot{V} = \frac{1 - A^2}{1 + A^2} UW - V, \tag{2.13}$$

$$\dot{W} = \frac{A^2 - B^2}{A^2 + B^2} UV. \tag{2.14}$$

(For the remainder of §2 the letter $B$ will be used to denote the aspect ratio and should not be confused with the strength of the magnetic field.) This nonlinear system has a number of remarkable properties. The nonlinear terms conserve the total kinetic energy and the total angular momentum

$$E = \tfrac{1}{2}[(1 + B^2)U^2 + (1 + A^2)V^2 + (A^2 + B^2)W^2], \tag{2.15}$$

$$L = (1 + B^2)^2 U^2 + (1 + A^2)^2 V^2 + (A^2 + B^2)^2 W^2. \tag{2.16}$$

The magnetic field gives rise to an anisotropic damping, embodied in the linear dissipative terms on the right-hand side of equations (2.12) and (2.13). The total kinetic energy obeys

$$\frac{\mathrm{d}E}{\mathrm{d}t} = -\mu \tag{2.17}$$

where $\mu = (1 + B^2)U^2 + (1 + A^2)V^2$ is the rate of Joule dissipation. As a result, the kinetic energy of the flow will always decay unless it is in a purely two-dimensional motion perpendicular to the magnetic fied ($U = V = 0, W \neq 0$). Observe that the electromagnetic interaction parameter $N$ (cf. equation (1.1)), which is commonly used in the analysis of MHD turbulence and represents the ratio between the eddy turnover time and Joule damping time, does not appear in the system because we have used the Joule time scale $\alpha^{-1}$ to non-dimensionalize the vorticity coefficients. Instead, the non-dimensional values of $U$, $V$, and $W$ represent the order of magnitude of $1/N$. Our approach here is similar to the one using the vorticity-based definition (1.3) of the interaction parameter. When the ellipsoid is axisymmetric around the axis of the magnetic field ($A = B$), the component of the angular momentum parallel to the magnetic field is an additional conserved quantity which imposes a constraint on the decay of energy. This property has been proven by Davidson (1997) for the case of a sphere and arbitrary initial conditions. It is however worth noting that our simple system does not only permit an easy derivation of this property but also admits a fully analytic solution to the decay problem, which can be readily worked out by taking $W = $ const. and solving the remaining linear problem for $U$ and $V$ in the axisymmetric case.

### 2.2. *Linear stability analysis of steady states*

Equations (2.12)–(2.14) admit a steady solution $(U, V, W) = (0, 0, W_0)$ describing two-dimensional motion perpendicular to the magnetic field. (Remember that the magnetic field is in the $z$-direction.) We analyse the stability of this solution by considering infinitesimally perturbed states of the form $(U, V, W) = (0, 0, W_0) + (\xi, \eta, \zeta)$ and

solving the linearized version

$$\dot{\xi} = -\xi + \left( \frac{B^2 - 1}{B^2 + 1} W_0 \right) \eta, \tag{2.18}$$

$$\dot{\eta} = \left( \frac{1 - A^2}{1 + A^2} W_0 \right) \xi - \eta, \tag{2.19}$$

$$\dot{\zeta} = 0, \tag{2.20}$$

of equations (2.12)–(2.14). Assuming that the perturbations depend on time as $(\xi, \eta, \zeta) = (\xi_0, \eta_0, \zeta_0) \exp(\lambda t)$ the solvability condition for the resulting linear algebraic system readily yields the growth rates in the form

$$\lambda_{1/2} = -1 \pm W_0 \sqrt{\frac{(A^2 - 1)(1 - B^2)}{(A^2 + 1)(1 + B^2)}}, \quad \lambda_3 = 0. \tag{2.21}$$

Instability occurs when $A > 1$, $B < 1$ or $A < 1$, $B > 1$, i.e. when the magnetic field is parallel to the middle axis of the ellipsoid and the $W$-component exceeds the critical value

$$W_c = \sqrt{\frac{(A^2 + 1)(1 + B^2)}{(A^2 - 1)(1 - B^2)}}. \tag{2.22}$$

In dimensional form (where $W$ has dimension s$^{-1}$) the result is

$$W_c = \frac{\sigma B^2}{\rho} \sqrt{\frac{(a^2 + c^2)(c^2 + b^2)}{(a^2 - c^2)(c^2 - b^2)}}. \tag{2.23}$$

When $a \to \infty$ and $b \to 0$ we have $W_c \to 1$ (non-dimensional) and $W_c \to \sigma B^2/\rho$ (dimensional) which implies that a very elongated structure becomes unstable when the interaction parameter defined as $N = \sigma B^2/\rho W$ becomes smaller than the critical value $N_c = 1$. For the purpose of comparison with the stability results for an unbounded elliptical vortex to be derived in §4, it is useful to rewrite the stability result (2.23) for the particular case $a = c\sqrt{E}$, $b = c/\sqrt{E}$ in terms of the eccentricity $E$ as

$$N_c = \left| \frac{E - 1}{E + 1} \right|. \tag{2.24}$$

The critical interaction parameter is unaffected by the exchange of the axes $a$ and $b$, i.e. $N_c(E) = N_c(E^{-1})$. For $E > 1$, $N_c$ is a monotonically increasing function of the eccentricity with $N_c \to 1$ as $E \to \infty$. The angle $\theta$ between the vorticity of the unstable mode and the direction of the magnetic field is equal to $\pi/2$. Observe that $W_0 > W_c$ is a sufficient condition for instability of the steady state but $W_0 < W_c$ does not imply its stability since the class of our perturbations is limited to the velocity fields described by equation (2.5).

The stability result (2.23) is unambiguous but its interpretation (2.24) in terms of the interaction parameter is not. This is because, as has already been discussed in §1.2, the definition of $N$ is not unique. It was suggested by one of the referees that the definition based on the actual magnitude of the vorticity $\boldsymbol{\omega}$ of the basic flow, namely

$$N^{vort} = \frac{\sigma B^2}{\rho \|\boldsymbol{\omega}\|} = \frac{\sigma B^2}{\rho (a/b + b/a) W}, \tag{2.25}$$

leads to a different conclusion. For this choice of $N$ the stability threshold (2.23) translates into

$$N_c^{vort} = \frac{E}{E^2 + 1} \left| \frac{E - 1}{E + 1} \right|. \tag{2.26}$$

The function $N_c^{vort}(E)$ is zero for $E = 1$, $E \to 0$ and $E \to \infty$ and attains a maximum value of approximately 0.15 at $E \approx 2.9$ (and by symmetry at $E \approx 1/2.9$). One could therefore argue that there is an optimal finite aspect ratio that is most unstable.

The instability that we have identified in this particular MHD problem is the elliptical instability, widely known in ordinary hydrodynamics. Its nature was extensively discussed by Kerswell (2002). In an unbounded domain it can be best understood as the result of a parametric resonance between Kelvin waves, existing due to the homogeneously rotating part of the velocity field, and the strain field, being a result of the elliptical shape of the streamlines. The elliptical instability is known to provide a fundamental mechanism in ordinary hydrodynamics for the transition to turbulence. Our stability results show that a magnetic field can suppress this instability. However, for any value of the magnetic field there are always flows (with $W > W_c$ in equation (2.23)) which are susceptible to the elliptical instability. It would be interesting to study the effect of viscosity and Hartmann boundary layers upon this instability. Unfortunately, this is not possible within a rigorous analytic framework. In the Appendix we show that the addition of phenomenological dissipative terms to the linear stability equations (2.18)–(2.20) leads to the conclusion that the critical velocity for rotation around the middle axis increases with viscosity whereas the (stable) rotation about the short or the long axis cannot be destabilized by viscosity.

### 2.3. *Nonlinear dynamics and the unstable character of purely two-dimensional motion*

Having identified the elliptical instability as a basic mechanism responsible for transforming a two-dimensional into a three-dimensional MHD flow, we wish to analyse the nonlinear evolution of the system. We focus our attention on the case where the initial state is an almost two-dimensional flow characterized by $U(0) \ll W(0)$ and $V(0) \ll W(0)$. A numerical solution of (2.12)–(2.14) for $A = 2$ and $B = 0.5$ shows that as long as $W(0) < W_c = 5/3$, i.e. the velocity is below its critical value, the system always relaxes to a purely two-dimensional state ($U = 0$, $V = 0$, $W < W_c$). Figure 2 shows that the evolution from an initial condition with $W(0) > W_c$ proceeds in a quite different way. Although the system finally settles into a purely two-dimensional state, the evolution towards this state is characterized by long periods of nearly two-dimensional motion, occasionally interrupted by violent three-dimensional transients. During these transients kinetic energy is fed from the non-dissipative two-dimensional mode $W$ to the three-dimensional modes $U$ and $V$ as can be seen in figure 2(c). The transients lead to a significant Joule dissipation of kinetic energy as is illustrated by the behaviour of the total kinetic energy and energy dissipation in figures 2(b) and 2(d), respectively. As a further illustration, figure 2(e) shows the solution trajectory in the phase space ($U, V, W$). The reversals of $W$ during the transients occur in turn in the $U = V$ and $U = -V$ planes. The periods of nearly stagnant two-dimensional behaviour correspond to the system residence near the upper and lower turning points. Such behaviour indicates that a decaying initially nearly two-dimensional MHD flow does not necessarily stay close to a two-dimensional form owing to the action of the elliptical instability. In figure 2(a) one might have expected that the reversals cease once the value of $|W|$ has fallen below the critical value $W_c = 5/3$.
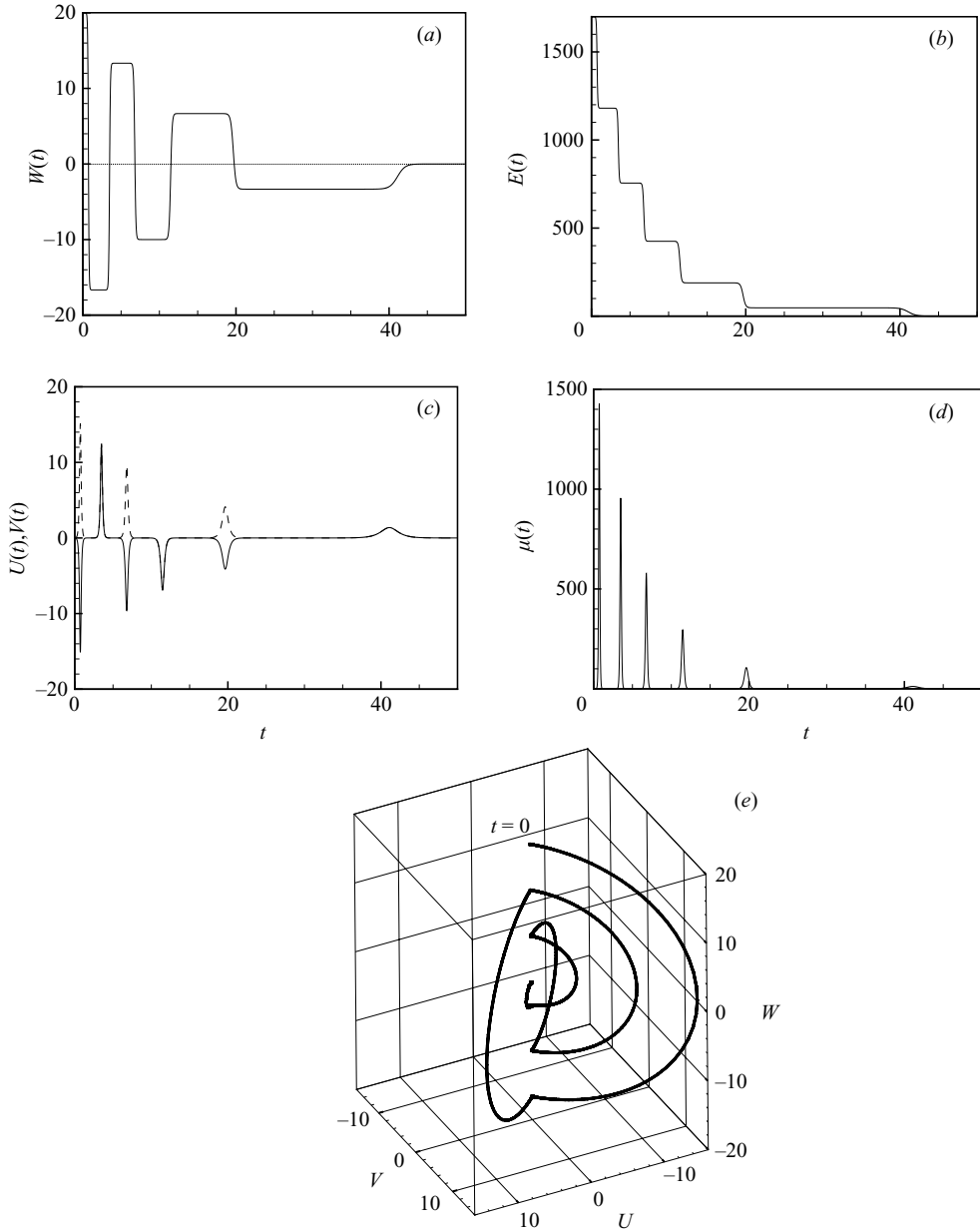
FIGURE 2. Decaying solution of (2.12)–(2.14). (*a*) Amplitude $W(t)$ of two-dimensional motion with vorticity parallel to the magnetic field. (*b*) Total kinetic energy (2.15). (*c*) Amplitudes $U(t)$ and $V(t)$ of motion with vorticity perpendicular to the magnetic field. (*d*) Rate of Joule dissipation $\mu$. Notice that the amplitude $W$ in the final state in (*a*) is small but non-zero. Its numerical value depends on the initial condition but obeys always $|W| < |W_c|$. (*e*) Phase trajectory of the solution.

The unstable character of purely two-dimensional evolution is further illustrated by slightly extending our model to include a phenomenological forcing term, which describes the application of an external torque parallel to the direction of the magnetic
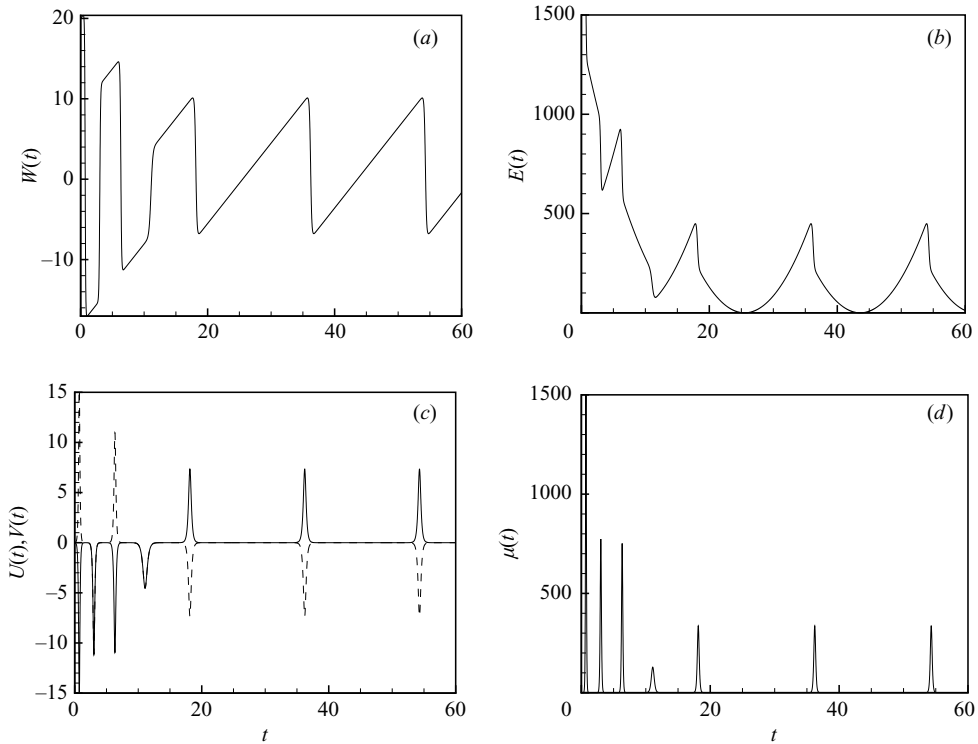
FIGURE 3. As in figure 2 but for the forced system (2.12), (2.13), (2.27). It may seem that the two-dimensional flow state persists at $W$ growing to much larger values than the linear stability limit $W_c = 5/3$ (see $a$ and $c$). In fact, the quasi-two-dimensional periods are characterized by slow evolution of small-amplitude $U$ and $V$, and the energy growth starts soon after $W$ crosses the stability threshold.

field. Equation (2.14) is thus replaced by

$$\dot{W} = \frac{A^2 - B^2}{A^2 + B^2} \, UV + 1. \tag{2.27}$$

The new model admits an exact two-dimensional solution

$$U = 0, \quad V = 0, \quad W = t, \tag{2.28}$$

whose kinetic energy grows monotonically with time and whose Joule dissipation is zero. However, the numerical solution computed from a weakly three-dimensional initial condition shows a completely different behaviour. The flow corresponding to the numerical solution shown in figure 3 is periodic in time and involves long-lasting periods of almost two-dimensional motion interrupted by strong three-dimensional excursions. Most importantly, the flow is 'statistically' steady in that the time-averaged kinetic energy does not change and the mean Joule dissipation is finite. The flow is therefore neither mathematically nor physically close to the two-dimensional behaviour suggested by the exact solution (2.28).

Although our simple model is only a caricature of the behaviour of real MHD turbulence, it allows us to draw a number of conclusions which serve as guidelines for the investigation of the full problem. In particular, we have learned that

(i) a purely two-dimensional MHD flow inside an ellipsoid is prone to the elliptical instability if $N \leqslant 1$ or $N^{vort} \leqslant 0.15$,

(ii) the nonlinear three-dimensional evolution of the elliptical instability leads to strong Joule dissipation,

(iii) an initially nearly two-dimensional flow does not necessarily stay close to purely two-dimensional evolution,

(iv) a decaying flow eventually arrives at a stable steady state,

(v) on the other hand, if the energy is supplied by an external forcing, such a stable state is never achieved and the flow remains in intermittent evolution indefinitely.

The intermittent behaviour of the model system with forcing is not unexpected and consistent with known behaviour of more realistic MHD flows. For example, simulations of forced MHD turbulence (Zikanov & Thess 1998) revealed a similar intermittent evolution with large-scale quasi-two-dimensional structures established under the action of the magnetic field only to become unstable and disintegrate shortly after that. On the other hand, the intermittency of decaying solutions shown in figure 2 is a new phenomenon for MHD flows observed for the first time in our model system.

## 3. Instability in an unbounded domain

For the further analysis it is convenient to write the basic equations (2.2) and (2.3) for the flow of a liquid metal in a homogeneous magnetic field at low magnetic Reynolds number in a more compact form as

$$\frac{\partial \boldsymbol{v}}{\partial t} + (\boldsymbol{v} \cdot \nabla)\boldsymbol{v} = -\frac{1}{\rho}\nabla p - \frac{\sigma B^2}{\rho}\Delta^{-1}\frac{\partial^2 \boldsymbol{v}}{\partial z^2}, \quad \nabla \cdot \boldsymbol{v} = 0. \tag{3.1}$$

Here $\Delta^{-1}$ is a symbolic notation for the solution of a Poisson equation of the form $\Delta \boldsymbol{a} = \boldsymbol{b}$ (with boundary condition $|\boldsymbol{a}(\boldsymbol{x})| \to 0$ for $|\boldsymbol{x}| \to \infty$) as $\boldsymbol{a} = \Delta^{-1}\boldsymbol{b}$ and the formulation (3.1) is entirely equivalent to (2.2) and (2.3) (Roberts 1967). We are interested in the stability of two-dimensional flows for which the Joule dissipation vanishes. The most general flow of this type is of the form

$$\boldsymbol{v}(x, y, t) = \boldsymbol{U}(x, y, t) + W(x, y, t)\boldsymbol{e}_z \tag{3.2}$$

where $\boldsymbol{U}$ has the properties $\boldsymbol{U} \cdot \boldsymbol{e}_z = 0$, $\nabla \cdot \boldsymbol{U} = 0$, and $\boldsymbol{U}$ and $W$ are solutions of

$$\frac{\partial \boldsymbol{U}}{\partial t} + (\boldsymbol{U} \cdot \nabla)\boldsymbol{U} = -\frac{1}{\rho}\nabla P, \tag{3.3}$$

$$\frac{\partial W}{\partial t} + (\boldsymbol{U} \cdot \nabla)W = 0. \tag{3.4}$$

The two terms in equation (3.2) describe the superposition of a two-dimensional motion perpendicular to the magnetic field with a motion parallel to the magnetic field.

Investigation of the stability of the general solution (3.2) is a formidable task (even in the inviscid case), as it would require consideration of the initial value problem (3.1) for all admissible fields $\boldsymbol{U}$ and $\boldsymbol{V}$. We shall simplify the task by considering two families of structures which we believe are representative of the solutions to (3.3) and (3.4), namely columnar vortices with elliptical streamlines and vortex sheets whose velocity is parallel to the direction of the magnetic field.

## 4. Instability of motion perpendicular to the magnetic field

### 4.1. *Linear stability of an elliptical vortex*

In order to anlyse the stability of two-dimensional motion perpendicular to the magnetic field, we consider an unbounded strained vortex described by

$$U(x, y) = -\Omega E y \, e_x + \Omega E^{-1} x \, e_y. \tag{4.1}$$

When the eccentricity $E = 1$, the flow is a solid-body rotation around the axis of the magnetic field with vorticity $2\Omega$. When $E > 1$, the flow has uniform vorticity $\omega = (E + E^{-1})\Omega$, uniform strain, and its streamlines are ellipses with semi-axes $a = \sqrt{E}$ and $b = 1/\sqrt{E}$, as can be readily inferred from the streamfunction

$$\psi = -\Omega \left( E \frac{x^2}{2} + E^{-1} \frac{y^2}{2} \right) \tag{4.2}$$

corresponding to (4.1). We extend the analysis of Bayly (1986) and Waleffe (1990) to the magnetic case by perturbing the basic flow (4.1) according to $v = U + u$. Linearizing (3.1) with respect to the perturbation we obtain the stability equation

$$\frac{\partial u}{\partial t} + (U \cdot \nabla)u + (u \cdot \nabla)U = -\frac{1}{\rho}\nabla p - \alpha \Delta^{-1} \frac{\partial^2 u}{\partial z^2}, \quad \nabla \cdot u = 0, \tag{4.3}$$

where $\alpha = \sigma B^2/\rho$. This system admits solutions of the form

$$u = \hat{u}(t) \cdot \exp\left[ i k(t) \cdot x - \alpha \int_0^t \frac{k_z^2(t')}{k^2(t')} dt' \right], \tag{4.4}$$

$$p = \hat{p}(t) \cdot \exp\left[ i k(t) \cdot x - \alpha \int_0^t \frac{k_z^2(t')}{k^2(t')} dt' \right], \tag{4.5}$$

where the unknown functions $\hat{u}(t)$, $\hat{p}(t)$, and $k(t)$ must be determined by enforcing the stability equation and incompressibility constraint (4.3). Inserting (4.4) and (4.5) into (4.3) we obtain

$$\dot{\hat{u}}_j + i\dot{k}_l x_l \hat{u}_j + ik_m A_{ml} x_l \hat{u}_j + A_{jl}\hat{u}_l = -ik_j \hat{p}, \quad k_j \hat{u}_j = 0, \tag{4.6a, b}$$

where $A_{12} = -\Omega E$, $A_{21} = \Omega/E$, and $A_{ij} = 0$ otherwise, are the components of the velocity gradient matrix. These equations are identical to those for the non-magnetic problem, solved by Bayly (1986) and Waleffe (1990). For the sake of completeness we repeat the main steps of their solution here. For details, however, we refer the reader to the original papers. Solvability of (4.6) requires that the terms independent of $x_l$ and proportional to $x_l$ balance each other separately. After elimination of the pressure, which is accomplished by a scalar product of (4.6a) with $k$, and incorporation of the incompressibility condition in the form $k_j \dot{\hat{u}}_j = -\dot{k}_j \hat{u}_j$ we are left with the stability equations

$$\dot{\hat{u}}_j = (2k^{-2}k_j k_l - \delta_{jl})A_{lm}\hat{u}_m, \quad \dot{k}_j = -k_l A_{lj}, \tag{4.7a, b}$$

which describe the evolution of the velocity perturbation and wavenumber with time. Equation (4.7b) is readily solved in the form $k(t) = k_0[\sin\theta \cos\phi(t),$ $E \sin\theta \sin\phi(t), \cos\theta]$ where $\phi(t) = \Omega(t - t_0)$ and $k_0$ and $t_0$ are integration constants. Here $\theta$ denotes the angle between the wavenumber and the magnetic field. With this explicit solution at hand, equation (4.7a) becomes a linear differential equation whose coefficients are periodic functions of time with periodicity $T = 2\pi/\Omega$. Floquet theory states that the general solution to such equations is a product of a function with exponential time dependence and a function which has the same periodicity as the

coefficients. Therefore the solution for $\hat{\boldsymbol{u}}(t)$ must be of the form $\hat{\boldsymbol{u}}(t) = e^{\lambda t}\boldsymbol{w}\,[\phi(t)]$ where $\boldsymbol{w}\,[\phi + 2\pi] = \boldsymbol{w}\,[\phi]$. We compute the growth rates $\lambda$ in the same way as Bayly (1986), who showed that they can be expressed in the form $\lambda(\Omega, E, \theta) = \Omega(2\pi)^{-1}\ln[\mu(E, \theta)]$ where the $\mu$ are eigenvalues of an auxiliary eigenvalue problem. With this step done, we can write down the amplitude of perturbations as $|\boldsymbol{u}(t)| = |\boldsymbol{w}(t)|\,\exp[F(t)]$, introducing the abbreviation

$$F(t) = \lambda(E, \theta, \Omega)t - \alpha \int_0^t \frac{\cos^2\theta\,\mathrm{d}t'}{\sin^2\theta\cos^2\Omega(t'-t_0') + E\sin^2\theta\cos^2\Omega(t-t_0') + \cos^2\theta}.$$
(4.8)

The second term on the right-hand side is the only correction to the non-magnetic solution. Reverting to dimensionless time $\phi = \Omega(t - t_0)$ and using a magnetic interaction parameter defined by

$$N = \alpha/\Omega = \sigma B^2/\rho\Omega$$
(4.9)

we can express $F$ as

$$F(\phi) = \frac{\phi}{2\pi}\ln[\mu(E, \theta)] - N\int_0^\phi \frac{\mathrm{d}\phi'}{1 + \tan^2\theta[\cos^2\phi' + E\sin^2\phi']}.$$
(4.10)

It is seen that the amplitude of perturbations does not have a purely exponential time dependence, in contrast to many common stability problems. This is a consequence of the anisotropic electromagnetic damping embodied in the last term of equations (4.8) and (4.10). A criterion for instability may nevertheless readily be formulated, since the integral in equation (4.10) is a periodic function of $\phi$. The system is unstable if $F$ increases over one period, i.e. $F(2\pi) - F(0) > 0$, it is stable if $F(2\pi) - F(0) < 0$, and the condition for neutral stability is therefore $F(2\pi) - F(0) = 0$. From the last condition we obtain the desired explicit expression for the neutral surface as

$$N(E, \theta) = \ln[\mu(E, \theta)]\left\{\int_0^{2\pi}\frac{\mathrm{d}\phi}{1 + \tan^2\theta[\cos^2\phi + E\sin^2\phi]}\right\}^{-1}.$$
(4.11)

To avoid confusion (because the word 'neutral' starts with 'N') we remind the reader that $N$ is (still) the magnetic interaction parameter defined by equation (4.9).

As was already discussed in §§ 1.2 and 2.2, we can introduce an alternative definition of the interaction parameter based on the actual vorticity of the basic flow, namely

$$N^{vort} = \frac{\sigma B^2}{\rho\|\omega\|} = \frac{N}{E + E^{-1}}.$$
(4.12)

In the next section we shall interpret the linear stability results both in terms of $N$ and $N^{vort}$.

## 4.2. *Stability results for the elliptical vortex*

Figure 4 shows the numerically computed values of the neutral interaction parameter as a function of $E$ and $\theta$. Observe that there is an intimate connection between the magnetic and the non-magnetic problem in that the interaction parameter of the critical magnetohydrodynamic mode is proportional to the growth rate of an unstable perturbation in the purely hydrodynamic problem. For $E = 1$ we have $N = 0$, indicating that a vortex with circular streamlines is always stable. The modes take the form of Kelvin waves which rotate about the magnetic field with a frequency $2\Omega\cos\theta$ (see e.g. Greenspan 1968).
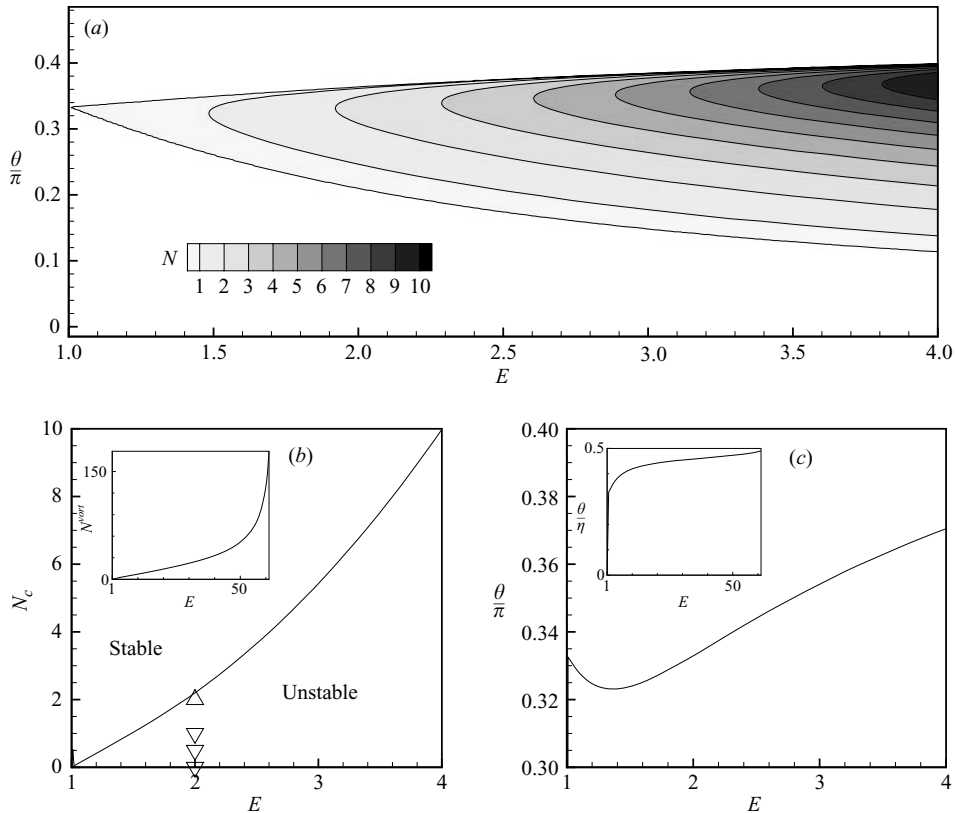
FIGURE 4. Stability of an unbounded strained vortex. (*a*) Neutral magnetic interaction parameter (4.11) as a function of eccentricity $E$ and angle $\theta$ between the wavenumber vector $\boldsymbol{k}$ of the perturbations and the axis of the vortex. (*b*, *c*) critical interaction parameter $N_c$ and $\theta_c$ as functions of $E$. $\triangledown$ and $\triangle$ in (*b*) show parameters, at which, respectively, instability and stability of a space-limited vortex is detected (see §4.3). Inset in (*b*) shows the behaviour of the vorticity-based interaction parameter introduced in (4.12). Inset in (*c*) is a plot of the critical angle over a wider range of eccentricities.

As soon as the eccentricity is non-zero, the flow becomes unstable with respect to perturbations located within a band $\theta_-(E) \leqslant \theta \leqslant \theta_+(E)$. Notice that the location of this unstable band is the same as in the non-magnetic problem since it is determined by the zeros of $\ln[\mu(E, \theta)]$. In particular, this band originates at $\theta = \pi/3$ (Bayly 1986), i.e. weakly elliptical unstable perturbations rotate around the magnetic field with the same frequency as the basic flow. For a given value of $E > 1$ the maximum of $N(E, \theta)$ over all $\theta$ in the unstable band defines the critical magnetic interaction parameter $N_c(E)$ and a critical angle $\theta_c(E)$. These quantities are plotted in figure 4(*b*, *c*). Figure 4*b* shows that $N_c$ increases rapidly with increasing eccentricity while the critical angle $\theta_c$ stays in the vicinity of $\pi/3$. The vorticity-based interaction parameter $N^{vort}$ is also a monotonically increasing function of the eccentricity, as can be verified by inspection of the inset in figure 4*b*. This is in contrast to the behaviour of $N^{vort}(E)$ for the triaxial ellipsoid which has maximum at $E \approx 2.9$, as was discussed in §2.2. The monotonic increase of the critical interaction parameter implies that strongly elliptical structures are particularly prone to instability. Having in mind that the nonlinear evolution of initially circular vortices governed by the

two-dimensional Euler equation (3.3) always leads to the generation of elliptical vortices, we can conclude that the two-dimensional evolution proceeds in such a way as to make the system more susceptible to the elliptical instability. Whether the elliptical instability is also relevant to the destabilization of strained vortex filaments which are characteristic of two-dimensional turbulence remains speculative (Kerswell 2002). The fact that $\theta_c \sim \pi/3$ may seem counterintuitive, as one usually expects in MHD that unstable structures have a tendency to align with the magnetic field ($\theta \to \pi/2$). However, it should be noticed that $\theta_c$ is monotonically, albeit slowly, increasing. We performed additional computations at $E$ up to 100 and found a clear indication that $\theta$ asymptotes towards $\pi/2$. The shape of the critical curve is qualitatively similar to that obtained analytically for the flow in the ellipsoid in §2 (equation (2.24)). However, in the latter problem we had $N_c \to 1$ as $E \to \infty$ reflecting the fact that the internal flow is more stable owing to its confined nature.

### 4.3. *Nonlinear instability of a finite elliptic vortex*

In this section, we complement the analysis of elliptic instability by three-dimensional nonlinear simulations of a horizontally spatially limited vortex. Understanding of the effect of finite size seems to be important because, as was demonstrated by Zikanov & Thess (1998), a forced turbulent flow in the presence of a strong magnetic field tends to develop quasi-two-dimensional strained vortices with typical horizontal size corresponding to the energy injection scale. It was also shown that the combined action of the elliptic instability and Joule dissipation can result in an intermittent quasi-two-dimensional–three-dimensional behaviour not unlike the intermittency obtained in §2 of this paper for a model system.

The non-magnetic precursor of our simulations is the work by Lundgren & Mansour (1996), who consider transition to turbulence in a swirling flow confined in a box $0 \leqslant x \leqslant L_x = \pi/b_1$, $0 \leqslant y \leqslant L_y = \pi/b_2$, $0 \leqslant z \leqslant L_z$ with impermeable sidewalls and periodicity in the $z$-direction. The basic flow is two-dimensional with the streamfunction

$$\Psi = A \frac{\sin b_1 x \sin b_2 y}{b_1^2 + b_2^2}, \tag{4.13}$$

and vorticity

$$\omega = A \sin b_1 x \sin b_2 y. \tag{4.14}$$

The streamlines given by (4.13) are nearly elliptical in the central part of the box with the eccentricity $E = L_x/L_y$. The flow is not affected by a vertical magnetic field and is an exact solution of the Euler equations.

It was shown by Lundgren & Mansour (1996) that the instability of (4.13) to infinitesimal three-dimensional perturbations is qualitatively similar to that of an unbounded uniform vortex (4.1). Quantitative similarity (close stability limits and critical wavenumbers) can, in principle, be achieved if one considers perturbations with high wavenumber $k \to \infty$. In real numerical simulations, this limit can never be attained. Moreover, as demonstrated below, the wavelengths of the most energetic growing modes are comparable with the horizontal size of the vortex. The average vorticity of the non-dimensional basic flow

$$\langle \omega \rangle = A(L_x L_y)^{-1} \int_0^{L_x} \int_0^{L_y} \omega \, \mathrm{d}y \, \mathrm{d}x \tag{4.15}$$

is, therefore, a more relevant measure of vorticity, presumably serving the purpose of comparison with the linear theory developed for an infinite vortex better than the

peak vorticity $\omega(L_x/2, L_y/2)$. For this reason, in the simulations, we use the vorticity amplitude $A = \pi^2/4$, which provides the average vorticity $\langle\omega\rangle = 1$.

The flow can be conveniently simulated using one of the pseudospectral codes designed for DNS of turbulent flows in a periodic box. The code can be based on a sine-transform or, if the numerical resolution is not an issue, a full fast Fourier transform. In the latter approach, which we follow, symmetries are enforced on the initial conditions so that four identical flows are calculated in the domain $2L_x \times 2L_y \times L_z$ with impermeable boundaries at $x = L_x$ and $y = L_y$.

We consider an incompressible low-$Rm$ MHD flow

$$\frac{\partial \boldsymbol{v}}{\partial t} + (\boldsymbol{v} \cdot \nabla)\boldsymbol{v} = -\nabla p - N\Delta^{-1}\frac{\partial^2 \boldsymbol{v}}{\partial z^2}, \quad \nabla \cdot \boldsymbol{v} = 0. \tag{4.16}$$

The vortex dimensions are $L_x = 2\pi$, $L_y = \pi$, $L_z = 4\pi$, which implies eccentricity $E = 2$. The magnetic interaction parameter is defined as $N = \sigma B^2/\rho$ based on $\langle\omega\rangle$ as the scale for $L/U$.

The viscosity term with $Re = 10^6$ is added to the momentum equation in the calculations with the purpose of controllable removal of spurious small-scale oscillations. Such a high value of $Re$ results in a scenario maximally close to the inviscid linear instability considered in the previous section. The resulting viscous dissipation is negligibly weak, probably weaker than the artificial numerical dissipation of the scheme. Both kinds of dissipation are active only at the smallest resolved scales of the flow.

This 'pseudo-inviscid' approach is different from the approach of Lundgren & Mansour (1996) who used moderate values of $Re$ and studied the entire process of transition to a turbulent state. The rationale is that the focus of our analysis is on the first stages of the nonlinear evolution of the instability, which is characterized by the concentration of energy in the large-scale modes (the base flow and the unstable eigenmodes with few subharmonic modes generated by their nonlinear interaction). At sufficiently high Reynolds number, this evolution is dominated by the elliptic instability and magnetic dissipation. The role of viscosity is negligible. The results presented below only concern these first stages. In order to guarantee that they are unaffected by inadequately resolved small-scale dynamics we monitor the two-dimensional (in the $k_\perp, k_z$-plane) energy spectra and stop the simulations as soon as the first noticeable excitation of the small scales is observed.

The effective numerical resolution (number of degrees of freedom used for one vortex) is $N_x \times N_y \times N_z = 64 \times 32 \times 128$. The initial velocity perturbations added to the basic flow at $t = 0$ are random fields that satisfy the incompressibility conditions and have the energy power spectrum

$$E(k) = 10^{-6}k^4 \exp[-2(k/2)^2]. \tag{4.17}$$

Four numerical experiments with $N = 0$, 0.5, 1, and 2 are presented below. The evolution of global characteristics of the flow is illustrated in figure 5. A good indicator of the stability is growth/decay of the average kinetic energy of the parallel (vertical) velocity component, which is absent in the basic flow. One can clearly see in figure 5(a) that the magnetic field suppresses the instability. The vortex is unstable at $N = 0$, 0.5, and 1, but stable at $N = 2$. This is in qualitative agreement with the results of linear stability analysis of an infinite vortex as illustrated in figure 4(b). The growth rate of the perturbations clearly decreases with $N$. The evaluation based on the quasi-exponential portions of the $E_3(t)$ curves yields 0.25, 0.18, and 0.09, for $N = 0$, 0.5, and 1, respectively.
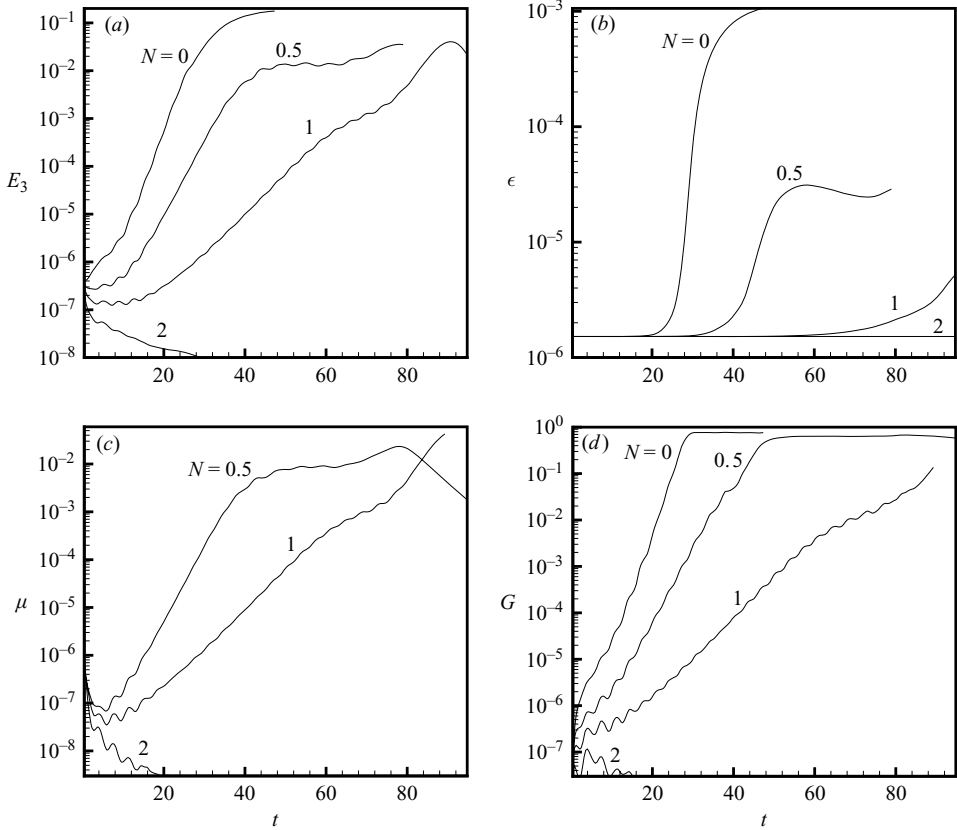
FIGURE 5. Nonlinear instability of a limited elliptic vortex. (*a*) Perturbation kinetic energy $E_3(t)$ of the parallel velocity component. (*b*) Rate of viscous dissipation $\epsilon(t)$. (*c*) Rate of Joule dissipation $\mu(t)$. (*d*) Anisotropy coefficient (4.18.)

As further characteristics of the evolving three-dimensional perturbations, spatially averaged rates of viscous and Joule dissipation are shown in figure 5(*b*,*c*) as functions of time. We also show, in figure 5(*d*), the characteristic of the anisotropy of the flow gradients

$$G = \frac{\langle(\partial u/\partial z)^2\rangle}{2\langle(\partial u/\partial x)^2\rangle}. \tag{4.18}$$

The coefficient $G$ is zero in a two-dimensional flow that does not depend on the $z$-coordinate (for example, the basic vortex) and unity in an isotropic flow. Use of this coefficient follows the earlier simulations of MHD turbulence of Zikanov & Thess (1998) and Schumann (1976). The necessity for the factor 2 in the denominator becomes obvious if one considers the kinematic property of the isotropic velocity spectrum (Hinze 1959)

$$\left\langle \frac{\partial u_i}{\partial x_n}\frac{\partial u_j}{\partial x_m}\right\rangle = \frac{E}{\lambda}[\delta_{ij}\delta_{mn} - \tfrac{1}{4}(\delta_{in}\delta_{jm} + \delta_{im}\delta_{jn})],$$

where $u_i$ are the velocity components, $E$ is the energy, and $\lambda$ is the Taylor microscale.

The unstable flow behaviour shown in figure 5(*a–d*) can be explained on the basis of the interaction between evolving instability, with its energy transfer to smaller
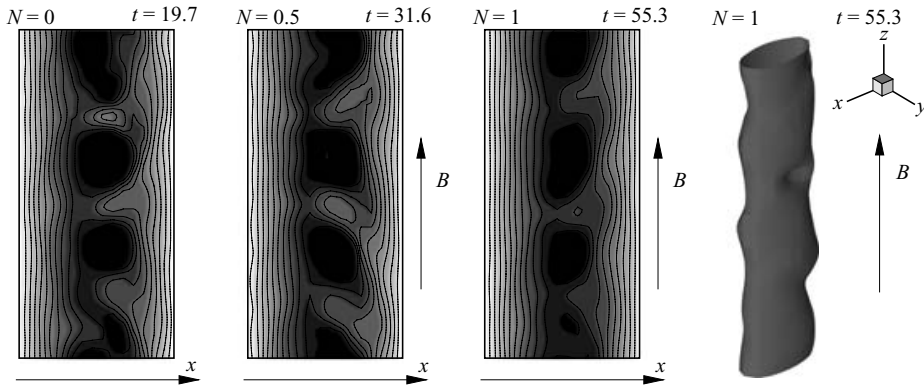
FIGURE 6. Instability of a limited elliptic vortex. Contours of the module of vorticity in the cross-section $y = \pi/2$ through the centre of the vortex and iso-surface of $|\omega| = 1.5|\omega|_{mean}$ are shown. Times are chosen so as to correspond to approximately equal stages of flow evolution.

scales and increasing three-dimensionality, and magnetic field. First and foremost, the Joule dissipation delays the transition. Furthermore, as one can conclude from the fact that the viscous dissipation rates achieved at late stages of transition decrease significantly with growing $N$, the presence of magnetic field prevents development of sharp velocity gradients.

Of interest is the behaviour of three-dimensionality characteristics, such as $G$ in figure 5($d$). At linear and early nonlinear stages of the evolution, they grow steadily. The absolute growth rate is smaller at higher $N$ but it seems that different flows taken at similar stages of evolution have comparable values of $G$. As the flow approaches nonlinear saturation, its dimensional anisotropy, as expressed by $G$, stabilizes at approximately constant levels. Although it is difficult to recognize in figure 5($d$), these levels are quite different with and without magnetic field. For $N = 0$, we have $G \approx 0.75$ and for $N = 0.5$, $G \approx 0.6$. No reliable estimate can be obtained at $N = 1$ but $G$ never exceeds 0.15.

The spatial structure of the unstable flow during early stages of evolution is illustrated in figure 6. One can see that the magnetic field does not produce any dramatic changes. The perturbations at $N = 0.5$ and $N = 1$ do seem to be more elongated in the vertical direction than the perturbations at $N = 0$, but the effect is weak. The dominating wavelengths are also comparable.

The conclusion that a moderately strong magnetic field does not significantly modify the structure of instability modes is confirmed by the two-dimensional energy spectra shown in figure 7. The energy is concentrated in approximately the same modes at all three values of the magnetic interaction parameter. Moreover, we see that these modes follow closely the prediction of the linear theory for an infinite vortex (cf. figure 4$c$). Their wavenumbers lie close to the lines corresponding to the angle $\theta = \pi/3$ between the wavenumber vector and the magnetic field.

The absence of noticeable dependence of the instability modes on $N$ was consistently observed in all our numerical experiments. Remember, however, that the simulations were limited to early stages of the transition. At later stages, when the flow becomes truly three-dimensional and turbulent, the Joule dissipation is expected to play a more significant role.
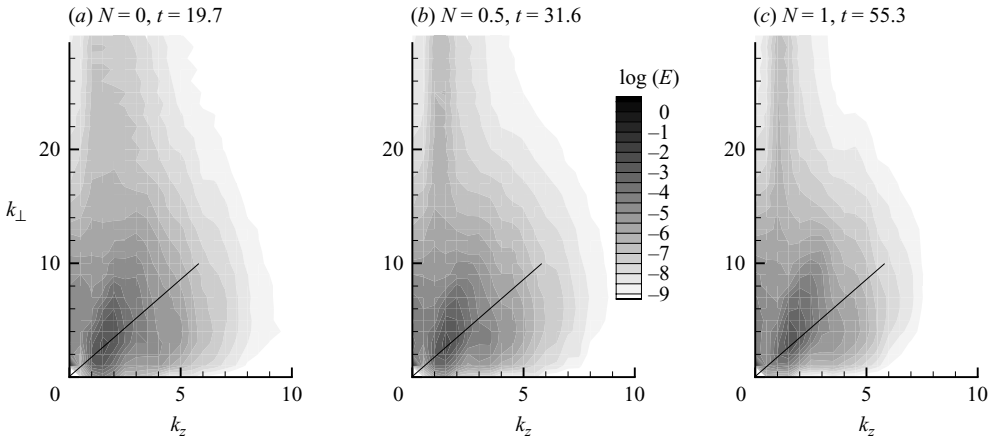
FIGURE 7. Instability of a limited elliptic vortex. Two-dimensional power spectra of perturbation kinetic energy. Lines corresponding to $\theta = \pi/3$ are shown for comparison.

## 5. Instability of motion parallel to the magnetic field

### 5.1. *Linear stability of a vortex sheet of zero thickness*

In purely two-dimensional flow the velocity component parallel to the magnetic field behaves like a passive scalar, transported by the velocity $U(x, y, t)$, cf. equation (3.4). Such evolution is known to produce steep gradients of $W(x, y, t)$ (see e.g. Kraichnan & Montgomery 1980; Lesieur 1990). In a real two-dimensional flow these gradients would be carried around and stretched which makes their general analysis difficult and their stability properties complex. However, since the archetype of such structures is a single vortex sheet, which is known to undergo a Kelvin–Helmholtz instability, we will discuss the stability of the flow

$$W(x) = U_0 \frac{x}{|x|} \tag{5.1}$$

under the influence of the parallel magnetic field. This problem, along with more general unidirectional velocity fields, was originally considered by Drazin (1960). However, the spatial structure of the unstable modes were not investigated there and is therefore the central focus of the discussion given below.

The stability of infinitesimal perturbations $\boldsymbol{v} = (ik\hat{\psi}(x), 0, -d\hat{\psi}/dx)\exp[ik(z - ct)]$ (where $\hat{\psi}(x)$ is the $x$-dependent part of the two-dimensional complex-valued streamfunction $\hat{\Psi}(x, z)$) superimposed upon the basic flow (5.1) is determined by the third-order polynomial equation

$$-ic(1 + c^2) + \tfrac{1}{4}N(1 + 3c^2) = 0 \tag{5.2}$$

where $N = \sigma B^2/\rho U_0 k$ is the magnetic interaction parameter defined according to (1.4), and space and time are non-dimensionalized using $k^{-1}$ and $U_0 k$, respectively. The normal mode for $x > 0$ is given by

$$\hat{\psi}(x) = \exp\left(-x\sqrt{1 - i\frac{N}{c - 1}}\right) \tag{5.3}$$

where it is assumed that the square root with the positive real part has been taken.

Drazin (1960) has demonstrated that all three solutions of equation (5.2) are purely imaginary and that one of the solutions always has positive imaginary part, but he did
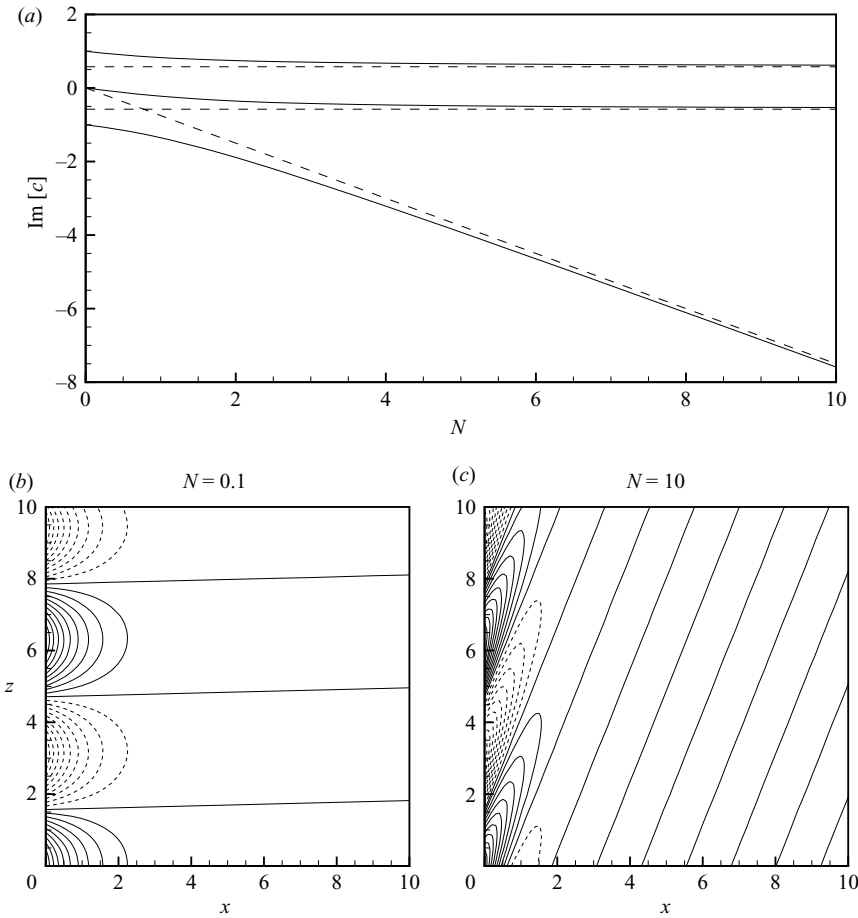
FIGURE 8. Instability of a vortex sheet. (*a*) Solution of the dispersion equation (5.2) (dashed lines are asymptotics for $N \to \infty$). (*b*) Streamfunction of the unstable mode at $N \ll 1$ (5.4). (*c*) Streamfunction of the unstable mode at $N \gg 1$ (5.5). In (*b*, *c*) solid (dashed) lines show positive (negative) values.

not explicitly calculate $c(N)$ and $\hat{\psi}(x)$. Figure 3(*a*) shows the imaginary parts of all three solutions as a function of $N$. Notice that the wavenumber $k$ does not explicitly appear in the solution because it represents the only characteristic length scale of the problem and has therefore been used to non-dimensionalize the equations. However, the wavenumber enters the definition of $N$.

For each value of $N$ there are two stable and one unstable solutions. When $N = 0$ we recover the classical Kelvin–Helmholtz instability with $c = i$. For $N > 0$ the imaginary part of the solution originating from $c = i$ always remains positive which implies that the vortex sheet is unstable for arbitrarily strong magnetic fields, although the growth rate decreases with $N$. The asymptotic behaviour of the wave velocity is $c = i(1 - N/4)$ for $N \ll 1$ and $c = i/\sqrt{3}$ for $N \gg 1$. The spatial structure of the unstable modes is best revealed by the two-dimensional (real-valued) streamfunction $\psi(x, z, t) = Re\{\hat{\Psi}(x, z)\} = Re\{\hat{\psi}(x) \exp[i(z - ct)]\}$ (non-dimensional variables) which, for a fixed time $t = 0$, is readily evaluated as

$$\psi(x, z) = \exp\left[-\left(1 + \tfrac{1}{4}N\right)x\right] \cos\left[-\tfrac{1}{4}Nx + z\right] \tag{5.4}$$

for $N \ll 1$ and as

$$\psi(x, z) = \exp\left[-3^{1/4}\left(\tfrac{1}{8}N\right)^{1/2}x\right]\cos\left[-3^{3/4}\left(\tfrac{1}{8}N\right)^{1/2}x + z\right] \qquad (5.5)$$

for $N \gg 1$. The streamfunctions are shown in figures 3($b$) and 3($c$). The unstable modes for large interaction parameter have an aspect ratio $z/x \sim N^{1/2}$ as is characteristic of MHD flows in strong magnetic fields.

## 5.2. *Stability of a vortex sheet of finite thickness*

The analysis of the previous section is valid only in the limit of infinitely large wavelengths. At finite wavelength, the thickness of the vortex sheet must be taken into account and the non-dimensional wavelength $k$ becomes another parameter affecting the growth rate of the perturbations. For a consistent analysis, it is also desirable to consider the effect of finite Reynolds number since viscosity is required for formation of a vortex sheet of finite thickness.

It was shown by Hunt (1966) that a sufficiently strong magnetic field may result in the most unstable perturbations being three-dimensional. This phenomenon is addressed in the separate investigation of Vorobev & Zikanov (2007). Here we limit the analysis to the instability to two-dimensional (uniform in the spanwise direction) perturbations, i.e. to an extension of the results of previous section to the case of finite thickness. The effect of finite Reynolds number was also investigated by Vorobev & Zikanov (2007). While briefly describing this part of their results we focus the following discussion on the inviscid case.

Using the perturbation streamfunction $\hat{\psi}(x)$ introduced in the previous section we can write the non-dimensional Rayleigh equation as

$$(W - c)(\mathrm{d}^2\hat{\psi}/\mathrm{d}x^2 - k^2\hat{\psi}) - \hat{\psi}\,\mathrm{d}^2W/\mathrm{d}x^2 + \mathrm{i}Nk\hat{\psi} = 0, \quad \hat{\psi} \to 0 \text{ as } x \to \pm\infty, \qquad (5.6)$$

where we used the velocity at infinity $U_0$ and the half-width $\delta$ of the vortex sheet as the velocity and length scales. The basic velocity profile

$$W(x) = \mathrm{erf}\left(\tfrac{1}{2}\pi^{1/2}x\right) \qquad (5.7)$$

is used and the problem parameters are $N = \sigma B^2\delta/\rho U_0$ and the non-dimensional wavenumber $k$.

The problem is solved by a numerical method similar to that used by Betchov & Szewczyk (1963) for a non-magnetic counterpart of the problem. Far from the vortex sheet, at $|x| > L$, the basic velocity is approximately constant, $W = \pm 1$, so an exponential solution can be found. We discretize the equation within $-L < x < L$ using a finite-difference scheme of second order and apply a shooting procedure to determine the complex wave velocity $c$ as an eigenvalue that provides a numerical solution matching the asymptotic exponential solutions and their first derivatives at $x = -L$ and $x = L$. Parameter $L$ and the number of grid points are chosen for each $k$ so that their further increase does not affect the solution. We found that $L = 10$ (in non-dimensional units) and 2000 grid points were more than sufficient at $k > 0.01$, while larger values had to be taken at smaller $k$.

The results of calculations are presented in figures 9 and 10. One can clearly see in figure 9($a$) that increase of $N$ leads to suppression of the growth rate $\sigma = k\,\mathrm{Im}[c]$ and to reduction of the range of unstable wavenumbers $k$. To investigate the asymptotic behaviour at $N \to \infty$, we calculate, at $0 \leqslant N \leqslant 100$, the maximum growth rate $\sigma_{max} = \max_k[\sigma(k)]$, the wavenumber $k_{max}$, at which this maximum occurred, and the wavenumber $k_{lim}$ such that all modes with $k > k_{lim}$ are stable. One can see in figures 9($b$) and 9($c$) that the magnetic field never fully suppresses the instability.
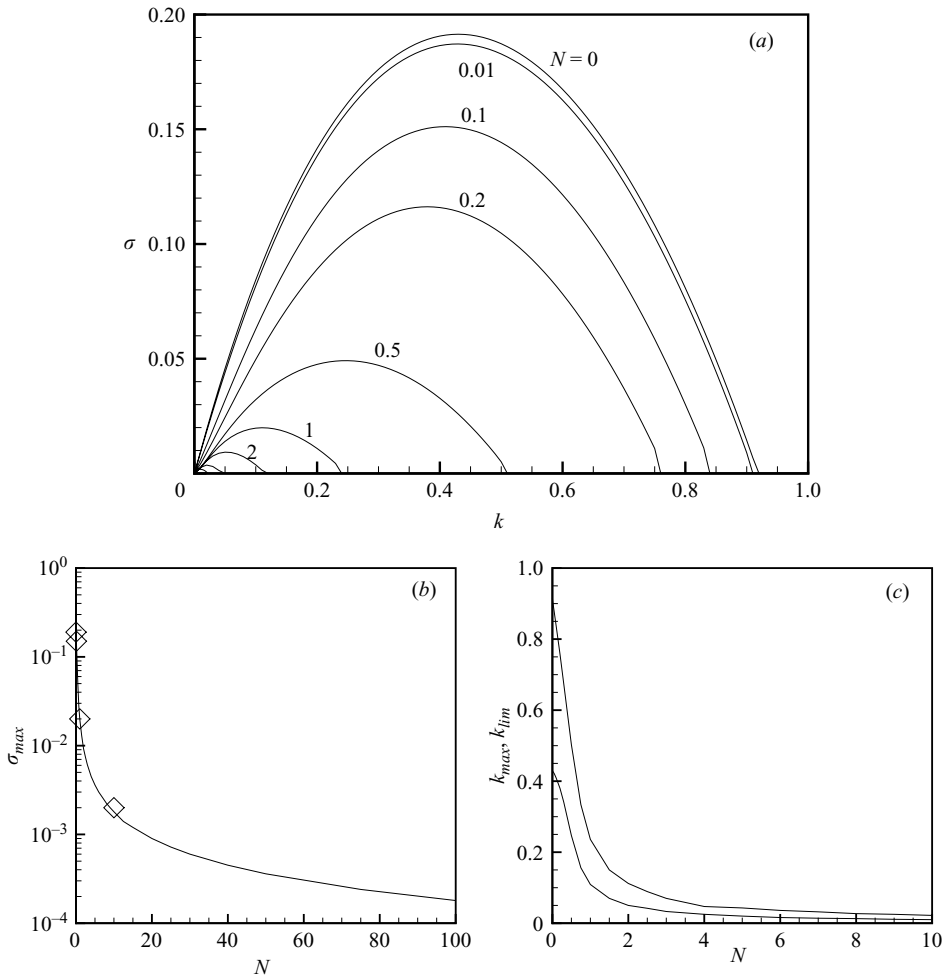
FIGURE 9. Instability of a vortex sheet of finite thickness. (*a*) Growth rate $\sigma = k\,\mathrm{Im}[c]$ as a function of the wavenumber $k$ for different magnetic interaction parameters $N$. Unmarked curves at bottom left correspond to $N = 5$ and $N = 10$. (*b*) The maximum growth rate $\sigma_{max}$ as a function of $N$; $\diamond$ mark the growth rates determined from nonlinear simulations. (*c*) The wavenumbers $k_{max}$, and $k_{lim}$ as functions of $N$.

There always exists a range of small wavenumbers, where the vortex sheet is unstable to, albeit slowly, growing perturbations. This result is not surprising as it reflects the simple fact that longer waves generate weaker velocity gradients and, thus, are less susceptible to the suppression by the magnetic field. At very large wavelengths, the low-$Rm$ approximation ceases to be valid and our analysis has to be replaced by the one based on the full MHD equations.

The agreement between the calculations and the analytical results for an infinitely thin sheet in §5.1 was verified by calculating $\mathrm{Im}[c]$ at $k$ as small as $10^{-5}$ for two cases, $N = 0$ and $N = 10$. It was confirmed that the numerical results converged, correspondingly, to $c = \mathrm{i}$ and $c = \mathrm{i}/\sqrt{3}$.

The main difference between the inviscid results presented in figure 9 and the results obtained by Vorobev & Zikanov (2007) in the case of finite Reynolds number
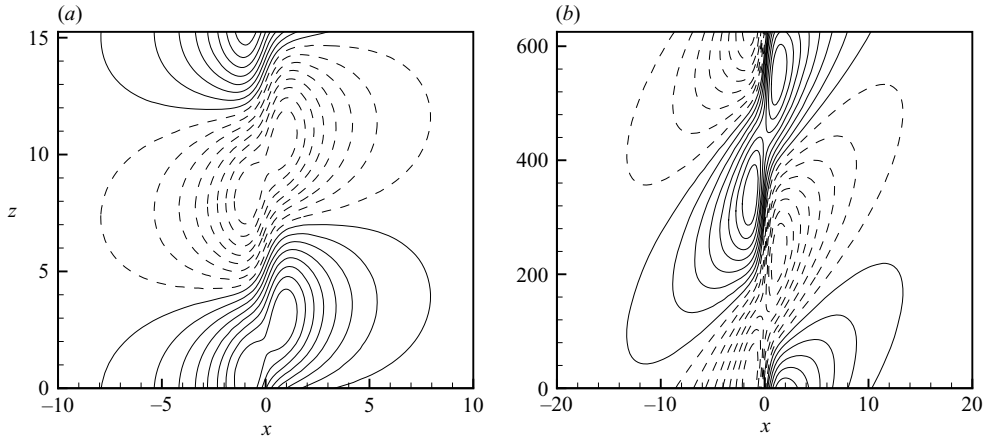
FIGURE 10. Instability of a vortex sheet of finite thickness. Streamfunctions of the unstable modes at (*a*) $N = 0.1$ and $k = 0.41$ and (*b*) $N = 10$ and $k = 0.01$. Solid (dashed) lines are used for positive (negative) values of the streamfunction. Note completely different $x$- and $z$-axis scales of the two pictures.

is in the behaviour of long-wave perturbations. At finite $Re$, the magnetic field stabilizes the modes with not only large but also small $k$. This has been observed at $10 \leqslant Re \leqslant 400$ and $N > 0$. While suppression at high $k$ is clearly consistent with our inviscid results and, in general, with the mechanism of magnetic dissipation of strong velocity gradients, the suppression at low $k$ does not seem to have a simple physical explanation. An important consequence of this modification is that, in the presence of viscosity, a sufficiently strong magnetic field with $N > N_{crit}(Re)$ can completely suppress the growth of two-dimensional perturbations. This is not in contradiction to our inviscid results since $N_{crit} \to \infty$ as $Re \to \infty$.

The spatial structure of the unstable inviscid modes is illustrated in figure 10(*a*, *b*). The modes with $k = k_{max}(N)$ are shown at low ($N = 0.1$) and high ($N = 10$) values of the interaction parameter. Note different aspect ratios of the two pictures. The structure in figure 10(*b*) is much more elongated in the direction of the magnetic field than the structure in figure 10(*a*). If we recalculate the magnetic interaction parameter with the wavelength as the length scale, the values corresponding to figures 10(*a*) and 10(*b*) will be 0.244 and 1000, respectively. The streamfunctions, therefore, represent the finite-thickness counterparts of the streamfunctions shown in figures 8(*b*) and 8(*c*).

To finalize the discussion of the Kelvin–Helmholtz instability we illustrate the nonlinear development of the two-dimensional inviscid unstable waves. The non-dimensional governing equations are

$$\frac{\partial \boldsymbol{v}}{\partial t} + \boldsymbol{v} \cdot \nabla \boldsymbol{v} = -\nabla p - N u \boldsymbol{e}_x, \quad \nabla \cdot \boldsymbol{v} = 0, \tag{5.8}$$

where $\boldsymbol{u} = (u, w)$ is the velocity field and $p$ is the pressure. The Lorentz force in the two-dimensional case is easily derived by taking the divergence of Ohm's law (equation (2.3)) which yields $\nabla^2 \phi = (\nabla \times \boldsymbol{u}) \cdot \boldsymbol{B}$. Since the vorticity is perpendicular to the magnetic field, the right-hand side of this equation vanishes and we have $\phi = 0$, from which it follows that $\boldsymbol{J} \times \boldsymbol{B} = \sigma (\boldsymbol{u} \times \boldsymbol{B}) \times \boldsymbol{B} = -\sigma B^2 u \boldsymbol{e}_x$. This formula renders the mechanism of instability suppression particularly transparent. Normal velocity perturbations associated with the wave induce electric currents in the spanwise
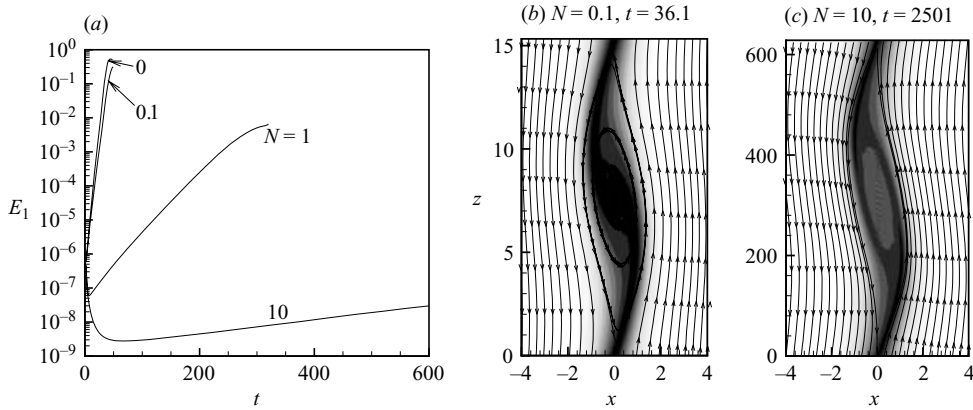
FIGURE 11. Nonlinear evolution of vortex sheet instability. (*a*), Kinetic energy $E_1$ of normal velocity component is shown as a function of time for simulations with different values of magnetic interaction parameter. (*b*, *c*), Streamlines and vorticity are shown for approximately equal stages of evolution at $N = 0.1$ (*b*) and $N = 10$ (*c*). Note completely different *z*-axis scales of the two pictures.

direction $j = B_0 \sigma u$, which interact with the imposed magnetic field to generate the returning force.

The problem is solved numerically in a manner similar to the earlier studies of non-magnetic instability (see e.g. Patnaik, Sherman & Corcos 1976). The initial conditions consist of the background shear flow (5.7) superimposed with a weak perturbation in the form of a single wave of the most unstable wavelength $\lambda = 2\pi / k_{max}$ and the spatial shape given by (5.4) or (5.5). The non-dimensional amplitude of the perturbation velocity is $10^{-3}$.

The computational domain is rectangular with size $\lambda$ and periodic boundary conditions in the streamwise direction. In the normal direction, both component of the perturbation velocity vanish at the boundaries $x = \pm L$, where $L$ is chosen large enough so that the artificial conditions do not affect the evolution of instability.

The numerical method is an adaptation of the method applied earlier by Zikanov, Slinn & Dhanak (2003) for simulation of a turbulent Ekman layer. The spatial discretization is a combination of the Fourier pseudo-spectral method in the streamwise direction and the second-order finite-difference scheme in the normal direction. The grid is clustered in the shear layer using the coordinate transformation $x = L \sinh(D\zeta) / \sinh(D/2)$, where $D$ is the parameter that determines the degree of clustering. The time-marching scheme is the explicit time-splitting method based on the third-order Adams–Bashforth algorithm with variable time step.

The last comment concerns the viscosity. As in the case of a finite elliptic vortex considered in §4.3, we limit the simulations to the first stages of the nonlinear instability of a flow with $Re \to \infty$, i.e. in the case of negligible viscous dissipation. Although a nominal viscous term is added to the equations, the Reynolds number is set to $10^6$ (so that the numerical dissipation is apparently stronger than the viscous) and the two-dimensional spectrum is monitored to stop the computations as soon as the small scales become populated.

The results are presented in figure 11(*a*, *b*). Four cases are considered, with $N$ equal to 0, 0.1, 1, and 10, and the perturbation wavenumber equal to $k_{max}(N)$, which is 0.43, 0.41, 0.11, and 0.01, respectively. The evolution of growing unstable modes is

illustrated in figure 11($a$) by the behaviour of the average kinetic energy $E_1 = (1/2)\langle u^2 \rangle$ of the velocity component $u$ normal to the direction of magnetic field and basic flow. The curves also represent the average Joule dissipation rates, which, in this particular case, are given by $\mu = 2NE_1$. The initial drop of the perturbation amplitude is soon replaced by nearly exponential growth, the rate of which is greatly affected by the magnetic field. The growth rates $\sigma$ evaluated on the basis of the exponential parts of the curves are in good agreement with the linear theory (see figure 9$b$).

The typical flows with growing billows are shown in figure 11($b$) for the cases of small ($N = 0.1$) and large ($N = 10$) magnetic interaction parameters. One can see that the anatomy of a two-dimensional flow does not principally change under the action of the magnetic field. We observe the same pattern of 'cat's eye' core and stretched 'braids' as in the well-documented non-magnetic case (see e.g Patnaik *et al.* 1976). The only significant effect of the magnetic field is the dramatic growth of the aspect ratio of the billows resulting from the growth of the unstable wavelength. One must note, of course, that this conclusion is limited to the early nonlinear stages of the transition. Other features of flow structure may be strongly affected by the magnetic field at late two-dimensional and three-dimensional stages.

## 6. Summary and conclusions

We have conducted several studies directed toward answering the question of whether a purely two-dimensional turbulent flow of an electrically conducting fluid described by equation (3.1) is stable with respect to three-dimensional perturbations when it is subjected to a uniform magnetic field. Instead of solving the full time-dependent problem for arbitrary flows (a hardly feasible task) we restricted our attention to a model MHD flow in a triaxial ellipsoid and to linear instability and subsequent nonlinear evolution of two prototype problems, namely a single elliptic vortex and a shear layer.

By formulating and solving an exact low-dimensional model for the flow in an ellipsoid we were able to provide evidence for the unstable character of purely two-dimensional MHD flows. The nonlinear evolution illustrated, with a simple example, another typical feature of MHD flows, the intermittent behaviour with long periods of quasi-two-dimensional motion interchanging with violent three-dimensional bursts.

The linear stability analysis of the unbounded elliptical vortex showed that this object is susceptible to the elliptical instability for an arbitrarily strong magnetic field provided the eccentricity (strain) is sufficiently large. The nature of the instability is not changed by the imposed magnetic field and remains that of the elliptic instability to modified Kelvin waves. The effect of the magnetic field is to moderate the growth of the unstable modes and to change the orientation of the neutral modes. The angle between their wavenumber vector and the axis of the vortex increases with $N$. The threshold of the instability and the form of the unstable perturbations was found to be in agreement with the results of fully nonlinear three-dimensional simulations of finite elliptic vortices.

The stability analysis of a free shear layer affected by a parallel magnetic field showed that this flow is also unstable at arbitrary strength of the magnetic field. This result was obtained at zero viscosity both for a vortex sheet and for a shear layer of finite thickness. The analysis was limited to spanwise-uniform perturbations. We found that the imposed magnetic field reduces the growth rate of the unstable modes but is unable to fully suppress the instability. There always remains a range of sufficiently large wavelengths in which the basic flow is unstable. The results of

the linear analysis were extended to two-dimensional nonlinear simulations of the evolution of unstable flow.

Our study does not provide an unambiguous answer to the main question formulated at the beginning of this paper, namely, whether or not the purely two-dimensional flow represents the high-field limit of three-dimensional MHD flows. It does, however, show that a two-dimensional turbulent flow can become unstable in the presence of an arbitrary strong magnetic field by forming unstable structures, such as strongly strained elliptic vortices or thin vortex sheets. It is impossible to predict, in the general case, the subsequent evolution of this flow. One of the possibilities realizable in a forced flow situation is transition to a statistically steady anisotropic MHD flow with a finite level of electromagnetic energy dissipation. Another is an intermittent evolution as illustrated by our model flow in a triaxial ellipsoid.

One should be wary of drawing conclusions from inviscid stability analysis without consideration of viscosity. A similar apparent paradox was encountered in the analysis of the magnetorotational instability (Velikhov 1959; Chandrasekhar 1960; Balbus & Hawley 1991, 1998) in differentially rotating fluids. Although mediated by a magnetic field, the instability seemed to persist in the limit of arbitrarily small field strength. The paradox was resolved by the realization that the unstable wavelengths become shorter and shorter as the field strength decreases, so in reality viscosity and resistivity provide a cutoff (Dubrulle & Knobloch 1992, 1993; Goodman & Ji 2002).

In the present problem one might think that the role of the viscosity is to damp the three-dimensional instabilities at small scales so that the strong-field limit would result in purely two-dimensional motion. However, the interplay of electromagnetic and viscous energy dissipation here is more subtle. Viscosity is indeed capable of providing a cutoff to the transverse wavenumbers $k_\perp$ but it cannot prevent the two-dimensional flow from radiating energy into the Joule cone sketched in figure 1. As long as the system is unbounded in the $z$-direction, any increase of the magnetic field will just lead to an increase of the wavelength of unstable modes while maintaining the electromagnetic energy dissipation. At the present time it is impossible to say in which situations and in what way this scenario will evolve. One counterexample is provided by Vorobev & Zikanov (2007) who showed that the combined action of viscosity and magnetic field can stabilize the long-wave perturbations of a free shear layer. In order to comprehensively understand the role of the two dissipation mechanisms, it would be necessary to fully extend the present stability analyses to the viscous case.

It would be interesting to study the properties of strongly anisotropic MHD flows by performing experiments on grid-generated turbulence in liquid metals (similar to those by Alemany *et al.* 1979; Caperan & Alemany 1985) but in magnetic fields of the order of 5 T. With Reynolds numbers of the order $Re \sim 10^6$ (implying magnetic Reynolds numbers $Rm \sim 0.1$) one would get close to the limit of validity of the quasistatic approximation ($Rm \ll 1$) but would still be greatly beyond the capabilities of direct numerical simulations.

## Appendix. The role of viscosity in the triaxial ellipsoid

In the presence of viscosity the flow in the ellipsoid can no longer be described exactly by a three-dimensional model such as (2.12)–(2.14). This is because the presence of Hartmann boundary layers at the walls cannot be captured by the simple velocity field given in equation (2.5). However, we can qualitatively explore the role of viscosity if we generalize the linear stability equations (2.18)–(2.20) to include weak dissipation in the form

$$\dot{\xi} = -(1 + \alpha)\xi + \left(\frac{B^2 - 1}{B^2 + 1} \, W_0\right) \eta, \tag{A 1}$$

$$\dot{\eta} = \left(\frac{1 - A^2}{1 + A^2} \, W_0\right) \xi - (1 - \beta)\eta, \tag{A 2}$$

$$\dot{\zeta} = -\gamma \zeta. \tag{A 3}$$

Here $\alpha$, $\beta$ and $\gamma$ are phenomenological damping parameters which are proportional to the viscosity of the fluid. Carrying out the same analysis as in §2.2 we obtain, after some algebra, the growth rates

$$\lambda_{1/2} = -1 - \left(\frac{\alpha + \beta}{2}\right) \pm \sqrt{W_0^2 \frac{(A^2 - 1)(1 - B^2)}{(A^2 + 1)(1 + B^2)} + \left(\frac{\alpha - \beta}{2}\right)^2}, \quad \lambda_3 = -\gamma. \tag{A 4}$$

If the rotation of the basic flow is around the middle axis, the critical $W$-component becomes

$$W_c = \sqrt{\frac{(A^2 + 1)(1 + B^2)}{(A^2 - 1)(1 - B^2)}(1 + \alpha)(1 + \beta)}. \tag{A 5}$$

Thus, the critical velocity given by equation (2.22) increases with increasing viscosity, implying that viscosity stabilizes the elliptical instability. If the rotation is about either the short or the long axis of the ellipsoid, one might expect that the previously stable solution could become unstable due to the viscosity. The situation is similar to the free rotation of a rigid body about a fixed point in which the stable solution of maximum energy (for given angular momentum) can be destabilized by arbitrarily weak dissipation. In the present case, however, a straightforward analysis leads to the result that in the cases $A < 1$, $B < 1$ and $A > 1$, $B > 1$ the system cannot become unstable.

## REFERENCES

ALEMANY, A., MOREAU, R., SULEM, P. L. & FRISCH, U. 1979 Influence of external magnetic field on homogeneous MHD turbulence. *J. Méc.* **18**, 280–313.

BALBUS, S. A. & HAWLEY, J. F. 1991 A powerful local shear instability in weakly magnetized disks. I. Linear analysis. *Astrophys. J.* **376**, 214–233.

BALBUS, S. A. & HAWLEY, J. F. 1998 Instability, turbulence, and enhanced transport in accretion disks. *Rev. Mod. Phys.* **70**, 1–53.

BAYLY, B. J. 1986 Three-dimensional instability of elliptical flow. *Phys. Rev. Lett.* **57**, 2160–2163.

BETCHOV, R. & SZEWCZYK, A. 1963 Stability of a shear layer between parallel streams. *Phys. Fluids* **6**, 1391–1396.

CAPERAN, P. & ALEMANY, A. 1985 Homogeneous low-magnetic-Reynolds-number MHD turbulence - Study of the transition to the quasi-two-dimensional phase and characterization of its anisotropy. *J. Méc.* **4**, 175–200.

CHANDRASEKHAR, S. 1960 The stability of non-dissipative Couette flow in hydromagnetics. *Proc. Natl Acad. Sci. USA* **46**, 253–257.

DAVIDSON, P. A. 1997 Magnetic damping of jets and vortices. *J. Fluid Mech.* **336**, 123–150.

DAVIDSON, P. A. 1999 Magnetohydrodynamics in Materials Processing. *Annu. Rev. Fluid Mech.* **31**, 273–300.

DAVIDSON, P. A. 2001 *An Introduction to Magnetohydrodynamics.* Cambridge University Press.

DORMY, E., CARDIN, P. & JAULT, D. 1998 MHD flow in a slightly differentially rotating spherical shell, with conducting inner core, in a dipolar magnetic field. *Earth Planet. Sci. Lett.* **160**, 15–30.

DORMY, E., JAULT, D. & SOWARD, A. M. 2002 A super-rotating shear layer in magnetohydrodynamic spherical Couette flow. *J. Fluid Mech.* **452**, 263–291.

DRAZIN, P. G. 1960 Stability of parallel flow in a magnetic field at small magnetic Reynolds number. *J. Fluid Mech.* **8**, 130–142.

DUBRULLE, B. & KNOBLOCH, E. 1992 On the local stability of accretion disks. *Astron. Astrophys.* **256**, 673–678.

DUBRULLE, B. & KNOBLOCH, E. 1993 On instabilities in magnetized accretion disks. *Astron. Astrophys.* **274**, 667–674.

GLEDZER, E. B., DOLZHANSKY, F. V. & OBUKHOV, A. M. 1981 *Systems of Hydrodynamic Type and their Applications.* Nauka, Moscow (in Russian).

GLEDZER, E. B. & PONOMAREV, V. M. 1977 Finite dimensional approximations of the motions of an incompressible fluid in an ellipsoidal cavity. *Isv. Atmos. Ocean. Phys.* **13**, 565–569.

GREENSPAN, H. P. 1968 *The Theory of Rotating Fluids.* Breukelen Press, Brookline.

GOODMAN, J. & JI, H. 2002 Magnetorotational instability of dissipative Couette flow. *J. Fluid Mech.* **462**, 365–382.

JIMENEZ, J. 1990 Transition to turbulence in two-dimensional Poiseuille flow. *J. Fluid Mech.* **281**, 295–297.

HINZE, J. O. 1959 *Turbulence.* McGraw-Hill.

HOLLERBACH, R. & SKINNER, S. 2001 Instabilities of magnetically induced shear layers and jets. *Proc. R. Soc. Lond.* A **457**, 785–802.

HUNT, J. C. R. 1966 On the stability of parallel flows with parallel magnetic fields. *Proc. R. Soc. Lond.* A **293**, 342.

KERSWELL, R. R. 2002 Elliptical instability. *Annu. Rev. Fluid Mech.* **34**, 83–113.

KNAEPEN, B. & MOIN, P. 2004 Large-eddy simulation of conductive flows at low magnetic Reynolds number. *Phys. Fluids* **16**, 1255–1261.

KRAICHNAN, R. H. & MONTGOMERY, D. 1980 Two-dimensional turbulence. *Rep. Prog. Phys.* **43**, 547–619.

LAHJOMRI, J., CAPERAN, P. & ALEMANY, A. 1993 The cylinder wake in a magnetic field aligned with the velocity. *J. Fluid Mech.* **253**, 421–448.

LESIEUR, M. 1990 *Turbulence in Fluids.* Kluwer.

LUNDGREN, T. S. & MANSOUR, N. N. 1996 Transition to turbulence in an elliptic vortex *J. Fluid Mech.* **307**, 43–62.

MOFFATT, H. K. 1967 On the suppression of turbulence by a uniform magnetic field. *J. Fluid Mech.* **28**, 571–592.

MOFFATT, H. K. 1978 *Magnetic Field Generation in Electrically Conducting Fluids.* Cambridge University Press.

MOREAU, R. 1990 *Magnetohydrodynamics.* Kluwer.

MUTSCHKE, G., GERBETH, G., SHATROV, V. & TOMBOULIDES, A. 2001 The scenario of three-dimensional instabilities of the cylinder wake in an external magnetic field: a linear stability analysis. *Phys. Fluids* **13**, 723–734.

NAKAUCHI, N., OSHIMA, H. & SAITO, Y. 1992 Two-dimensionality in low-magnetic Reynolds number magnetohydrodynamic turbulence subjected to a uniform external magnetic field and randomly stirred two-dimensional force. *Phys. Fluids* A **4**, 2906–2914.

PATNAIK, P. C., SHERMAN, F. S. & CORCOS, G. M. 1976 A numerical simulation of Kelvin–Helmholtz waves of finite amplitude. *J. Fluid Mech.* **73**, 215–240.

ROBERTS, P. H. 1967 *An Introduction to Magnetohydrodynamics*. Elsevier.

SCHUMANN, U. 1976 Numerical simulation of the transition from three- to two-dimensional turbulence under a uniform magnetic field. *J. Fluid Mech.* **74**, 31–58.

SOMMERIA, J. 1986 Experimental study of the two-dimensional inverse energy cascade in a square box. *J. Fluid Mech.* **170**, 139–168.

SOMMERIA, J. & MOREAU, R. 1982 Why, how, and when, MHD turbulence becomes two-dimensional. *J. Fluid Mech.* **118**, 507–518.

TSINOBER, A. 1990 MHD flow drag reduction. In *Viscous Drag Reduction in Boundary Layers* (ed. D. M. Bushnell & J. N. Hefner), pp. 327–349.

TSINOBER, A. 2001 *An Informal Introduction to Turbulence*. Kluwer.

VELIKHOV, E. P. 1959 Stability of an ideally conducting liquid flowing between cylinders rotating in a magnetic field. *Sov. Phys. JETP* **36** (9), 995–998.

VOROBEV, A. & ZIKANOV, O. 2007 Instability and transition to turbulence in a free shear layer affected by a parallel magnetic field. *J. Fluid Mech.* **574**, 131–154.

VOROBEV, A., ZIKANOV, O., DAVIDSON, P. A. & KNAEPEN, B. 2005 Anisotropy of magneto-hydrodynamic turbulence at low magnetic Reynolds number. *Phys. Fluids* **17**, 125105.

WALEFFE, F. A. 1990 On the three-dimensional instability of strained vortices. *Phys. Fluids* **2**, 76–80.

ZIKANOV, O., SLINN, D. N. & DHANAK, M. 2003 Large-eddy simulations of the wind-induced turbulent Ekman layer. *J. Fluid Mech.* **495**, 343–368.

ZIKANOV, O. & THESS, A. 1998 Direct numerical simulation of forced MHD turbulence at low magnetic Reynolds number. *J. Fluid Mech.* **358**, 299–333.